J Appl Physiol 125: 19–39, 2018.
First published February 15, 2018; doi:10.1152/japplphysiol.00842.2017.

INNOVATIVE METHODOLOGY

Measures of sympathetic and parasympathetic autonomic outflow from heartbeat dynamics

Gaetano Valenza,[1,5] Luca Citi,[2] J. Philip Saul,[3] and Riccardo Barbieri[4,5]

[1]*Computational Physiology and Biomedical Instruments Group, Bioengineering and Robotics Research Center E. Piaggio, and Department of Information Engineering, University of Pisa, Pisa, Italy;* [2]*School of Computer Science and Electronic Engineering, University of Essex, Colchester, United Kingdom;* [3]*Department of Pediatrics, West Virginia University School of Medicine, Morgantown, West Virginia;* [4]*Department of Electronics, Informatics and Bioengineering, Politecnico di Milano, Milano, Italy; and* [5]*Department of Anesthesia, Critical Care and Pain Medicine, Massachusetts General Hospital, Boston, Massachusetts*

Submitted 18 September 2017; accepted in final form 1 February 2018

Valenza G, Citi L, Saul JP, Barbieri R. Measures of sympathetic and parasympathetic autonomic outflow from heartbeat dynamics. *J Appl Physiol* 125: 19–39, 2018. First published February 15, 2018; doi:10.1152/japplphysiol.00842.2017.—Reliable and effective noninvasive measures of sympathetic and parasympathetic peripheral outflow are of crucial importance in cardiovascular physiology. Although many techniques have been proposed to take up this long-lasting challenge, none has proposed a satisfying discrimination of the dynamics of the two separate branches. Spectral analysis of heart rate variability is the most currently used technique for such assessment. Despite its widespread use, it has been demonstrated that the subdivision in the low-frequency (LF) and high-frequency (HF) bands does not fully reflect separate influences of the sympathetic and parasympathetic branches, respectively, mainly due to their simultaneous action in the LF. Two novel heartbeat-derived autonomic measures, the sympathetic activity index (SAI) and parasympathetic activity index (PAI), are proposed to separately assess the time-varying autonomic nervous system synergic functions. Their efficacy is validated in landmark autonomic maneuvers generally employed in clinical settings. The novel measures move beyond the classical frequency domain paradigm through identification of a set of coefficients associated with a proper combination of Laguerre base functions. The resulting measures were compared with the traditional LF and HF power. A total of 236 ECG recordings were analyzed for validation, including autonomic outflow changes elicited by procedures of different nature and temporal variation, such as postural changes, lower body negative pressure, and handgrip tests. The proposed SAI-PAI measures consistently outperform traditional frequency-domain indexes in tracking expected instantaneous autonomic variations, both vagal and sympathetic, and may aid clinical decision making, showing reduced intersubject variability and physiologically plausible dynamics.

NEW & NOTEWORTHY While it is possible to obtain reliable estimates of parasympathetic activity from the ECG, a satisfying method to disentangle the sympathetic component from HRV has not been proposed yet. To overcome this long-lasting limitation, we propose two novel HRV-based indexes, the sympathetic and parasympathetic activity indexes.

Address for reprint requests and other correspondence: G. Valenza, Bioengineering and Robotics Research Center E. Piaggio and Department of Information Engineering, University of Pisa, Largo Lucio Lazzarino 1, 56122 Pisa, Italy (e-mail: g.valenza@ieee.org).

autonomic nervous system; heart rate variability; Laguerre expansion; parasympathetic activity index; sympathetic activity index; sympathovagal balance

INTRODUCTION

Heartbeat dynamics and its spontaneous fluctuations are directly controlled by autonomic nervous system (ANS) outflow to the heart (34). Specifically, the multipath feedback system for neural control of the heart is manifested by the complex interaction between the sympathetic and parasympathetic (vagal) limbs of the ANS (44). Typically, for cardiovascular control, the sympathetic system is activated during the so-called "fight-or-flight" reactions, when there are drops in arterial pressure due to gravitational changes and during exercise, whereas the parasympathetic system predominates during a variety of resting conditions. The two systems generally act complementary, i.e., the increase of one usually corresponds to a decrease of the other. However, they present quite different temporal dynamics, mainly due to the different response properties of the two systems.

Sympathetic and parasympathetic activity interact to modify sinus node activity and produce the time-varying spontaneous variability of heart rate (HR), which is modulated by three major physiological factors: blood pressure control, thermal regulation, and respiration. Indeed, the cardiovascular homeostatic control is directed at maintaining arterial blood pressure according to peripheral blood flow demand.

Accordingly, in many cardiovascular diseases, abnormalities of autonomic cardiac control play an important role in the development and/or in the progression of the underlying pathological process. Examples include hypertension (18, 30), major depression (57), cirrhosis and ascites (16), obesity (15, 56), diabetes (13, 15), and heart failure (25, 36). Because the two systems might be differently affected by pathological outcomes, significant cardiovascular research has been focused on the reliable and effective assessment of the separate influences of parasympathetic and sympathetic neural pathways (2, 3, 19, 26, 32, 35, 37, 39, 41).

In this study, we present a novel parametric model of cardiovascular control, based on a specific combinatorial use of orthonormal Laguerre functions. This unique representation is

able to separately characterize sympathetic and parasympathetic activity by using only the timing of heartbeats. The rationale behind the proposed sympathetic activity index (SAI)-parasympathetic activity index (PAI) approach starts from the observation that the cholinergic and adrenergic drives have different temporal dynamics, partly overlapping in the frequency domain. For this reason, instead of base functions defined in limited frequency ranges (like the sinusoids for a simple frequency transform), a proper weighted sum and/or subtraction of primitives unselectively spanning the frequency domain would be able to decompose the heartbeat variability due to ANS activity by disentangling the unique contribution of each autonomic branch. Such primitives can be defined from discrete-time orthonormal Laguerre bases, which, for a given α, have equal magnitude and different phase spectra in the frequency domain (31, 33, 53).

Technically, heartbeat series are convolved through the Laguerre functions to identify personalized time-varying Laguerre coefficients, which are embedded in an autoregressive (AR) model combining the input data. Finally, a specifically tailored combination of the Laguerre coefficients defines two independent measures: the SAI and the PAI. According to the estimation method chosen to derive the Laguerre coefficients, it is possible to obtain finite SAI and PAI estimates within a given observation in time (e.g., by using least squares and maximum likelihood estimation methods), to obtain beat-to-beat SAI and PAI estimates in time (e.g., by using Kalman filtering), or to obtain instantaneous SAI and PAI estimates in time by using point-process modeling (7, 53).

The presented results are aimed at comparing the new definitions of ANS activity with current frequency-based methods in several electrocardiogram (ECG) studies involving sympathovagal modulations induced by postural changes (standing, slow tilting, and fast tilting) (53), selective autonomic blockade (42), lower body negative pressure (LBNP) (61, 62), and handgrip (61, 62).

We show experimental results on SAI, PAI, as well as low frequency (LF) and high frequency (HF) powers using time-varying estimates gathered from Kalman and point-process methods. When possible, we emphasize the use of point-process statistics for the SAI and PAI estimates because of several advantages (7, 53): *1*) from the event-related structure of the R-waves, this approach provides instantaneous heartbeat estimates in the time and frequency domains; *2*) it assesses the model goodness of fit (7, 53), i.e., how well a given model describes the observed R-R interval series; and *3*) there is no need for interpolation methods to be applied on the original R-R interval series. Note that our point-process modeling is based on a physiological plausible, history-dependent inverse Gaussian probability functions (7, 14, 53).

The paper is organized as follows: PHYSIOLOGY OF THE SYMPATHETIC AND PARASYMPATHETIC SYSTEMS AT A GLANCE briefly describes the fundamental physiology of the sympathetic and parasympathetic nervous systems; ESTIMATION METHODS OF SYMPATHETIC AND PARASYMPATHETIC PERIPHERAL OUTFLOW IN HUMANS reports on the current state of the art of estimation of ANS DYNAMICS FROM HEARTBEATS; DERIVATION OF THE NOVEL SYMPATHETIC AND PARASYMPATHETIC ACTIVITY MEASURES explains technical details on the SAI and PAI estimation based on Laguerre functions; EXPERIMENTAL SETUP and EXPERIMENTAL RESULTS describe data and results, respectively, related to the several experimental protocols employed for the measures validation.

PHYSIOLOGY OF THE SYMPATHETIC AND PARASYMPATHETIC SYSTEMS AT A GLANCE

The sympathetic and parasympathetic nervous systems are quite different functionally, anatomically, and physiologically. Both systems carry sensory (afferent) signals to the brain and spinal cord, and efferent signals from the brain to the target organs. The central nervous system (CNS) control comes mostly from the hypothalamus, with inputs also from the limbic system and the reticular activating system (47). The nucleus of the solitary tract in the medulla is the primary site of termination of cardiopulmonary afferents from cranial nerves involved in brain stem reflex control. Here, the connection between the CNS and its effector consists of two kinds of neurons: the preganglionic neuron and the postganglionic neuron. The synapses between these two neurons lie outside the CNS, in autonomic ganglia.

The parasympathetic system originates in the brain stem (cranial nerves III, VII, IX, and X) and sacral region of the spinal cord (S_2–S_4). The functions associated with this system are basically related to rest and digestive activity. Non-cardiopulmonary parasympathetic control is involved in salivation, production of digestive enzymes, peristalsis, urination, and defecation. Cardiopulmonary actions include reducing HR and blood pressure, reducing the respiratory rate, and conserving energy through relaxation and rest. The principal neurotransmitter is acetylcholine, released from both the preganglionic and the postganglionic neurons, and binding to cholinergic receptors. For the organism as a whole, the most important part of this system is the vagus nerve, which supplies parasympathetic signals to almost all of the organs of the thorax and abdomen.

The sympathetic system originates in the thoracic and lumbar regions of the spinal cord (T_1–L_2). The role of this system is related to the so called "fight-or-flight" response. Thus the sympathetic system prepares the body for situations requiring alertness or strength, or situations that arouse fear, anger, excitement, or embarrassment. In these kind of situations, the sympathetic nervous system may increase the HR, causes dilation of the bronchioles of the lungs (increasing oxygen intake), and contributes to dilation of blood vessels that supply the heart and skeletal muscles (increasing blood supply), while decreasing blood supply to organs not involved in the response (e.g., gut). The adrenal medulla is stimulated to release epinephrine (adrenaline) and norepinephrine (noradrenaline), which, in turn, increase the metabolic rate of cells and stimulate the liver to release glucose into the blood. Sweat glands are stimulated to produce sweat. The sympathetic nervous system afferents are also responsible for the transmission of visceral pain from organs such as the gut, bladder, and uterus.

Many functions of the sympathetic nervous system oppose those of the parasympathetic nervous system. Although it is noteworthy that not all organs receive innervation from both components of the ANS, it is quite often the case that multiple interactions between the two systems result in a nonlinear transmission of neural information to the organ of interest. A

good example of such interaction is evident in considering the autonomic outflow to the heart.

In fact, the sympathetic and parasympathetic branches, through their continuous dynamic interaction, modulate the HR response by means of the so-called bidirectional augmentation (46): during a predominant sympathetic control, a concomitant tonic vagal signal increases the gain of the transfer function relating dynamic sympathetic stimulation to HR, and vice versa (during a predominant parasympathetic control, a concomitant tonic sympathetic signal increases the gain of the transfer function relating dynamic vagal stimulation to HR). Such a bidirectional augmentation is mediated by cytosolic adenosine 3′,5′-cyclic monophosphate, which constitutes a component of the biological basis of nonlinear autonomic control on heartbeat dynamics.

ESTIMATION METHODS OF SYMPATHETIC AND PARASYMPATHETIC PERIPHERAL OUTFLOW IN HUMANS

Several methodologies for the assessment of sympathetic and parasympathetic activity in humans have been proposed throughout the past decades. Historically, measurement of plasma noradrenaline has represented a gold standard for the quantification of sympathetic neural functions (19). More recently, direct recording of sympathetic nerve activity via microneurography, direct catecholamine measurements, and noradrenaline radiotracer have largely supplanted the plasma noradrenaline approach (19). Neural imaging techniques also allow for direct visualization of sympathetic innervation of human organs, providing information on the in vivo metabolism of noradrenaline in different cardiovascular regions (19). However, such techniques require expensive equipment and technical support, and are not useful for assessing daily activities, as do devices such as a Holter monitor or other miniaturized wearable devices. Furthermore, power spectral density analysis of electrodermal activity has been recently proposed for the assessment of sympathetic functions (38).

Current autonomic estimates using HR variability and the frequency domain paradigm. Despite being widely introduced into the scientific practice and literature, the methods of autonomic activity evaluation noted above are not commonly used in clinical settings (19). Conversely, processing of HR data, commonly measured by detecting R-waves from the ECG, and the superimposed instantaneous heartbeat variations, referred to as HR variability (HRV) has been of growing importance in the attempt to develop real-time applications that use simple, noninvasive sensors in clinical and nonclinical settings (35, 39, 45). In fact, monitors of cardiovascular variability based on standard clinical multichannel signal acquisition equipment, single-channel miniature devices, smartphones, or wearable technology for ambulatory monitoring, have been effectively used in numerous settings, including the intensive care unit, the operating room, during normal daily activities, sleep, exercise, and during changes in emotional state or well-being states (see Refs. 35, 39, 41 for reviews, including many other applications).

From a technical point of view, the most widely used methodology to quantitatively assess ANS dynamics is based on a frequency-domain analysis, i.e., computing the HRV power spectral density (2, 3, 26, 35, 37, 39). Specifically, power in the HFs (0.15–0.4 Hz) of the HRV comprises respiratory-associated oscillations, which are mediated via the vagus nerve. Of note, the modulation of HR due to respiratory drive to cardiac vagal motoneurons refers to the so-called respiratory sinus arrhythmia (3, 35, 39, 65). Slower oscillations in the LFs (0.04–0.15 Hz) reflect to some extent slower closed-loop compensatory changes of blood pressure and HR mediated through the baroreflex and involving both autonomic branches (sympathetic and parasympathetic drive) (2, 3, 26, 35, 37, 39).

Specifically, the LF rhythm (centered at 0.1 Hz) of HRV is mainly due to arterial baroreflex modulation. It is also dramatically affected by the presence of vasomotor noise, which is amplified by the resonance in the baroreflex loop, placed around 0.1 Hz. Previous studies (1, 27, 29) suggested that the LF component of the power spectrum of HRV is strongly affected by the sympathetic system, as changes in the sympathetic gains cause a significant alteration in this component of the spectrum. However, it is clear that changes <0.15 Hz can be and are mediated by both cardiac vagal and sympathetic activity (42). Furthermore, recent evidences and meta-analyses point out how the HRV-LF band can be dramatically affected by parasympathetic dynamics (17, 40).

The HRV-HF components (>0.15 Hz) are determined by two concurrent mechanisms. The first is the effect of systemic arterial pressure changes mediated by the baroreflex. Such a pressure exhibits respiratory fluctuations caused by the intrathoracic and abdominal pressure changes (mechanical effect) and by the lung stretch receptor reflex working on resistance (neurogenic effect). These fluctuations systematically stimulate the baroreflex at the respiratory period. In this HF band, however, the baroreflex works entirely through its strong and fast vagal component, whereas the sympathetic component is almost completely suppressed because of its low-pass filtering dynamics. The second mechanism is due to a combination of the lung stretch receptor reflex effect on vagal activity and respiratory-related brain stem gating of vagal outflow. A common and widely accepted viewpoint in the literature is that the HF peak and power in the HRV-HF band can always be considered as a reliable index of vagal activity (17, 35, 39, 40, 50). Nevertheless, the HF peak is modulated by all factors affecting the input to baroreflex and the lung stretch reflex [such as the depth and frequency of breathing (22), venous compliances in the thoracic and abdominal cavity, posture changes (48), etc.] and depends strongly on the sensitivity of the cardiac pacemaker to efferent activity. Hence, as suggested by Akselrod (1) and Malpas (29), in different subjects and/or under different breathing conditions, the HF spectral component may be largely different, even in the presence of an equivalent vagal gain. Importantly, due to the mentioned ambiguity of the LF and HF power indexes, Malliani et al. (28) proposed the ratio of the LF power to HF power (hereinafter LF/HF) as an index of sympathovagal balance. Note that the use of LF/HF to assess the sympathetic and parasympathetic balance has also been challenged (17, 40).

Despite the mentioned references and its widespread use, HRV spectral analysis is far from being a definitive, reliable methodology for the noninvasive assessment of ANS functions. This has been known for more than 20 yr. As a matter of fact, a review on how to assess sympathetic activity in humans from Grassi and Esler (19) in 1999 reports that “the approach based on spectral analysis of HR and blood pressure signals has

been shown to have important limitations which prevent the method from faithfully reflecting sympathetic cardiovascular drive."

To date, standard HRV-based approaches have not been able to provide measures of autonomic activity, which overcome the large variability between normal subjects, thus limiting their use in clinical settings. A few investigations have attempted to overcome this significant limitation. Specifically, Vetter et al. proposed to quantify the ANS activity using a blind source separation technique of HR and blood pressure variability (58), as well using HR and QT-wave interval variability (59), whereas, more recently, Chen et al. (10) derived ANS activity indexes based on a multisignal analysis of the R-R variability by processing the HR, blood pressure, and the instantaneous lung volume. Similarly, Xiao et al. (63, 64) represented sympathetic and parasympathetic functions modeling the coupling mechanism between lung volume and HR. Although these sophisticated methods might have been successful in separating sympathetic and parasympathetic dynamics, they do require recordings of multiple physiological parameters to obtain the estimations.

Concerning the use of R-R interval series exclusively, Zhong et al. (66, 67) introduced a principal dynamic mode analysis of HRV to separately characterize the sympathetic and the parasympathetic activity. However, the authors reported that the algorithm requires proper calibration, and that a broadband HR spectrum is a strict requirement of such principal dynamic modes, a condition that may not be satisfied in some subjects (66).

To summarize, despite a few encouraging attempts, no methodology to date has been able to provide a separate, simultaneous, independent assessment of sympathetic and vagal instantaneous dynamics that can be *1*) obtained exclusively from the heartbeat, *2*) applied to a wide range of subjects, *3*) specifically tailored to the individual, and *4*) allowing for time-varying/instantaneous quantification (see Ref. 8 for review).

DERIVATION OF THE NOVEL SYMPATHETIC AND PARASYMPATHETIC ACTIVITY MEASURES

The "classic" frequency-domain characterization is based on the Fourier transform, an operator that represents HRV in the frequency space. The base functions of this space are defined by each sample along frequency. In the HRV case, these values are "grouped" by frequency range [very low frequency (VLF), LF, HF], as recommended in a 1996 guidelines document (35). The AR formulation has the property of reducing the dimensionality of the frequency space by defining a limited number of preferred oscillations (associated with the poles of the transfer function), dependent on the autoregression order. The variability related to each pole is then univocally associated to a specific frequency and can only be accounted for within each respective frequency range (again, VLF, LF, HF). This model has been of great success in many applications for autonomic assessment, as the frequencies/poles within the HF range have been directly associated with vagal dynamics in several instances. On the other hand, important limitations of such frequency subdivision have been recently pointed out (17, 19, 40), the most important being related to the fact that the LF range contains both vagal and sympathetic dynamics, and that respiratory dynamics shifts to the LF range would, consequently, affect the HF quantification of vagal influence. The primary rationale of this study is to overcome limitations imposed by the artificial separation of frequency ranges by defining a model whose base functions are not defined in the frequency domain, namely, Laguerre functions, which are a set of mathematical functions of time. Laguerre functions are characterized by a specific "order" (which can vary from zero to any other positive integer number), and a specific value "α," which characterizes fine modulation of the number of oscillations across zero, as well as very specific time responses. If we multiply two Laguerre functions of any order, the area under the curve is zero, a function of the property of "orthogonality." These functions are adopted as the base functions of a "new" Laguerre space.

The proposed SAI and PAI measures are derived characterizing and predicting each heartbeat event, given a combination of past information expressed as cardiovascular variability. Such formulation has been shown to improve the model parameter identification and reduce the number of parameters to be estimated (31, 33, 53).

Since the R-R intervals constitute the observation values used to estimate the model, the Laguerre-based characterization and prediction of heartbeat events by definition embed both sympathetic and parasympathetic information. Most importantly, the SAI collects a combination of Laguerre functions with slow responses (reflecting the slower conduction velocity associated with the sympathetic nerve), whereas the PAI combines contributions from Laguerre functions of higher order, thus representing responses along the entire frequency range (and not only HF, as in the standard spectral identification). As described below, a pharmacological autonomic blockade protocol was used as the training set to identify isolated dynamics. In this stage, extensive analysis was performed in confirming the effectiveness of the Laguerre-derived dynamics to separate the two cardiovascular autonomic outflows and, consequently, identify the best combinatorial coefficients.

Derivation methodology. As noted in the INTRODUCTION, the scientific rationale behind the hereby proposed measures of autonomic activity, SAI and PAI, relies on a proper combination of the so-called Laguerre coefficients, derived from the use of Laguerre functions, which have unique properties in the time and frequency domains, as well as in their high-order statistics (31, 33, 53).

Block schemes of all of the methodological stages involved in the SAI-PAI estimation are described in Figs. A3 and A4 of the APPENDIX.

The *j*th-order discrete-time orthonormal Laguerre function is defined as follows:

$$\phi_j(n) = \alpha^{\frac{n-j}{2}}(1-\alpha)^{\frac{1}{2}}\sum_{i=0}^{j}(-1)^i\binom{n}{i}\binom{j}{i}\alpha^{j-i}(1-\alpha)^i,\ (n \geq 0)$$

Figure 1 shows the first Laguerre functions for a given α value ($0 < \alpha < 1$), which determines the rate of exponential asymptotic decline of these functions.

Given a set of K heartbeat events, $\{u_k\}_{k=1}^{K}$ (e.g., R-waves from the ECG), let $RR_k = u_k - u_{k-1} > 0$ denote the kth R-R interval, or equivalently, the waiting time until the next R-wave event.

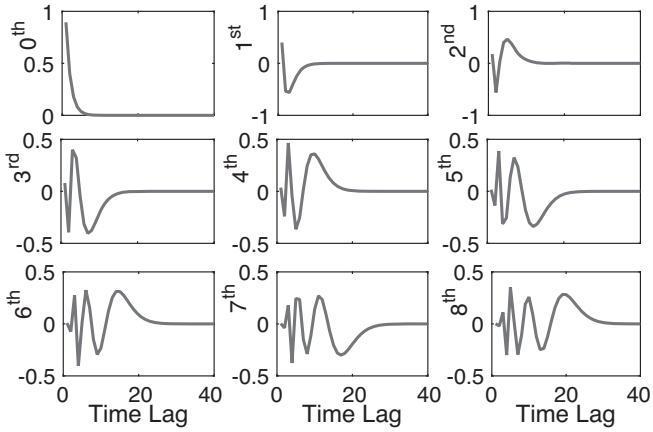

Fig. 1. Laguerre polynomials of order 8 for $\alpha = 0.2$ plotted over the first 40 lags.

Here, we propose to model heartbeat dynamics with μ_{RR} [t, $\mathcal{H}_t$, $\xi(t)$] at each time t as function of past R-R intervals, along with the Laguerre expansion. We take one step further and try to separate the influence of the sympathetic and parasympathetic system to the μ_{RR} [t, $\mathcal{H}_t$, $\xi(t)$] estimation. Hence:

$$\mu_{RR}\big[t, \mathcal{H}_t, \xi(t)\big] = g_0(t) + \underbrace{\sum_{j=0}^{P_{\text{Symp}}} g_1(j,t) l_j(t)}_{Sympathetic} + \underbrace{\sum_{j=P_{\text{Symp}}+1}^{P_{\text{ParSymp}}} g_1(j,t) l_j(t)}_{Parasympathetic} \quad (1)$$

where

$$l_j(t) = \sum_{n=1}^{\tilde{N}(t)} \phi_j(n) RR_{\tilde{N}(t)-n} \quad (2)$$

is the jth-order Laguerre filter output, and $\tilde{N}(t)$ denotes the index of the previous R-wave event occurred before time t, $\mathcal{H}_t = (u_k, \text{RR}_k, \text{RR}_{k-1}, ..., \text{RR}_{k-K+1})$ is the history of all previous R-R intervals before time t, and $\xi(t) = \{g_0(t), g_1(t)\}$ is the vector of the time-varying Laguerre coefficients to be estimated.

In an attempt to match the frequency response of the Laguerre filters with the dynamic response of the sympathetic and the parasympathetic systems (2, 3, 26, 35, 37, 39, 42), we have chosen $P_{\text{Symp}} = 1$ and $P_{\text{ParSymp}} = 8$. After preliminary testing on synthetic and experimental data (not shown), $\alpha = 0.2$ was chosen for the SAI and PAI derivation.

Finally, the definition of the SAI and PAI as a combination of disentangled Laguerre coefficients $\{g_1\}$ is as follows:

$$\text{SAI}\big[t, \xi(t)\big] = \Psi_{S_0} + \sum_{j=1}^{N_1} \Psi_{S_j} g_1(j-1, t) \quad (3)$$

$$\text{PAI}\big[t, \xi(t)\big] = \Psi_{P_0} + \sum_{j=1}^{N_2} \Psi_{P_j} g_1\big[j + (P_{\text{Symp}} + 1), t\big] \quad (4)$$

with $N_1 = P_{\text{Symp}} + 1$ and $N_2 = P_{\text{ParSymp}} - (P_{\text{Symp}} + 1)$.

Thanks to its parametric structure, the model-defined parameters can be updated along time using the most efficient and popular methods reported in recent literature for recursive parameter estimation.

However, by using point-process modeling, the Laguerre coefficients and, consequently, μ_{RR} [t, $\mathcal{H}_t$, $\xi(t)$], SAI [t, $\xi(t)$], and PAI [t, $\xi(t)$] can be defined in a continuous-time fashion, thus obtaining instantaneous autonomic activity measures at a very fine timescale with no interpolation between the arrival times of two beats.

In this study, the estimation of all model coefficients, including Laguerre coefficients $\{g_1\}$, was performed using a local maximum-likelihood estimation method. Additionally, model goodness of fit was based on the Kolmogorov-Smirnov (KS) tests and associated KS statistics (7). Particularly, the recursive, causal nature of the estimation allows for prediction of each new observation, given the previous history, independently at each iteration. The model and all of its parameters are, therefore, also updated at each iteration without priors. Autocorrelation plots were also utilized to test the independence of the model-transformed intervals (7). Exhaustive mathematical details on this matter are reported in the APPENDIX.

Optimal estimation of the Ψ_S and Ψ_P coefficients is a critical aspect in the proposed methodology. In fact, these values determine the capability of the algorithm to separate the sympathetic and parasympathetic components, both embedded in the disentangled Laguerre coefficients g_1. The Ψ_S and Ψ_P coefficients were obtained from respective sympathetic and parasympathetic blockades. Then, averaged values from subjects were fixed and used to obtain the linear impulse response functions from the Laguerre expansion approach.

To find unique Ψ_S and Ψ_P coefficients of broad applicability, i.e., suitable for a generic human subject, a specific a priori estimation was performed using a multiple linear regression technique on data involving selective autonomic blockade during postural changes (see Ref. 42 for experimental details). This data set was used as a training set by following the procedure, which is summarized as follows:

- ECG data were utilized from seven healthy subjects with atropine-induced parasympathetic blockade during a supine resting state and after a postural change by standing test.
- These data from each subject were used to derive the "purely" sympathetic coefficients $\{\Psi_S(j,n)\}_{n=1}^{N}$ by means of multiple linear regression considering a step function template having low value throughout the supine resting state, and high value throughout the standing phase after standing.
- Coefficients of general applicability for the sympathetic activity were then obtained through the average among subjects: $\{\Psi_{S_j}\} = \langle\{\Psi_S(j,n)\}_{n=1}^{N}\rangle_N$.

Likewise, the "purely" parasympathetic coefficients $\{\Psi_{P_j}\}$ were obtained by averaging among seven subjects using data gathered during sympathetic blockade, which was induced through a bolus of propranolol, and performing a multiple linear regression of a step function template having high value throughout the supine resting state, and low value throughout the standing phase after standing. Estimated coefficients are reported in *Working model coefficients* Ψ_S *and* Ψ_P below. Further test and validation data sets follow below.

EXPERIMENTAL SETUP

Autonomic activity measures were validated by analyzing an extensive collection of experimental ECG data, and comparing SAI, PAI, and their SAI-to-PAI ratio (SAI/PAI) with LF and HF power, and their LF/HF derived from standard frequency domain analyses. Experimental recordings were gathered during maneuvers that are well known in the literature to induce strong sympathovagal changes. These "gold-standard" studies for assessing autonomic activity are as follows: tilt-table protocols including *1*) stand up, *2*) slow tilt (i.e., 50 s from 0 to 70°), and *3*) fast tilt (i.e., 2 s from 0 to 70°); *4*) supine and standing during full autonomic blockade; *5*) LBNP test; and *6*) handgrip test.

Details on these experimental protocols follow below.

Tilt-table protocol. A single-lead ECG was continuously recorded from 10 healthy subjects undergoing a tilt-table protocol. Each subject was first placed horizontally in a supine position, with restraints used to secure him/her at the waist, arms, and hands. The subject was then tilted from the horizontal to the vertical position and returned to the horizontal position either through a "slow" tilt (50 s from 0 to 70°), or "fast" (i.e., 2 s from 0 to 70°). Stand-up sessions were also included.

The study was conducted at the Massachusetts Institute of Technology (MIT) General Clinical Research Center (GCRC) and was approved by the MIT Institutional Review Board and the GCRC Scientific Advisory Committee. Subjects were five men and five women: age 28.7 ± 1.2 yr (mean ± SD). Each subject performed six sessions (two stand up, two slow tilt, and two fast tilt) remaining in each upright state for 3 min. The protocol lasted 55–75 min (3,300–4,500 s).

Resting state is known to be associated with a dominant vagal activity, whereas states after tilting are known to be associated with a dominant sympathetic activity.

Full details on this experimental protocol can be found in Refs. 7, 20, 21, 53.

Lower body negative pressure. Fifty-eight healthy controls between 12 and 18 yr volunteered from schools in Oslo, Norway. Controls having a chronic disease (such as allergy) or using drugs (including contraceptive pills) on a regular basis were excluded for the study. One week before the experiments, all participants were instructed not to drink beverages containing alcohol or caffeine, not to take any drugs, and not to use tobacco products. They were instructed to fast overnight the day before the experiments. Written, informed consent was obtained from all participants and their parents. The study complied with the Declaration of Helsinki and was approved by the regional committee for ethics in medical research. Experiments started at 11 AM. The participants had been offered a light meal 2 h before, but were not allowed to eat or drink otherwise. They lay supine with their lower body in a plastic chamber from which air could be evacuated very rapidly, reaching a predefined negative pressure within milliseconds. They were familiarized with the test situations in two pilot experiments. Five minutes were used for baseline recording (resting state). Then LBNP of −20 mmHg was applied for 6 min. All subjects but one performed this procedure twice with continuous ECG recordings. Eight additional recordings were excluded from the analyses due to low technical quality; therefore, the total number of recordings used for this study was 106.

It is known that the resting state is associated with a dominant vagal activity, whereas the LBNP state is associated with a dominant sympathetic activity. Full details on this experimental protocol can be found in Refs. 61, 62.

Handgrip. The same subjects who performed the LBNP described in the previous paragraph also underwent a handgrip experimental procedure. Handgrip is a common test for studies of cardiovascular adjustments during isometric exercise. During handgrip, the cardiovascular adjustments are mainly due to CNS input to the baroreflex, thereby enhancing sympathetic neural activity.

Data used for this study included, for each subject, a 1-min segment before each handgrip (baseline) and a 1-min subsequent segment during handgrip with 30% of maximal voluntary contraction force (handgrip). Full details on this experimental protocol can be found in Refs. 61, 62.

Heartbeat correction and statistical analysis. To provide reliable results, all R-R-interval series must be free of algorithmic (e.g., from automatic peak detection procedure) errors and ectopic beats to avoid potential biases in statistical outcomes. To eliminate such anomalies, we preprocessed all heartbeat data with a previously developed real-time R-R interval error detection and correction algorithm based on the point-process statistics (local likelihood) (14). Visual inspection analysis of all HRV series was also carried out.

All analyses were performed using the Matlab software suite. Concerning descriptive statistics, for every subject and for every feature (SAI, PAI, SAI/PAI, LF power, HF power, and LF/HF) we condensed the information about the time-varying dynamics of feature through its median across time. Then, for each feature, we evaluated between-group differences using bivariate nonparametric statistics (Mann-Whitney or Wilcoxon test in case of unpaired or paired samples, respectively) under the null hypothesis that the between-subject medians of the two groups were equal.

Experimental results related to feature dynamics, presented in all of the figures and summary tables below, are condensed as median and its respective standard error based on the median absolute deviation (MAD) across subjects/recordings. This is consistent with the non-Gaussian distribution of some data samples ($P < 0.05$ from a KS normality test with null hypothesis of Gaussian distribution of data). Specifically, standard error was estimated as $1.4826\ \mathrm{MAD}(X)/\sqrt{n}$, where $\mathrm{MAD}(X) = \mathrm{Median}[|X - \mathrm{Median}(X)|]$, where X is the variable of interest (e.g., SAI, PAI, LF, HF, etc.), and n is the number of subjects in the data set of interest.

A P value of 0.05 was considered statistically significant.

EXPERIMENTAL RESULTS

From each single ECG recording, the R-R intervals were extracted using a curve length-based QRS detection algorithm (68). Then the resulting R-R interval series was visually inspected and eventually corrected through a previously developed error detection and correction algorithm (14). All recordings showed <5% of ectopic beats, and no significant algorithmic artifacts were detected.

The SAI-PAI validation was performed using the six experimental data sets described in EXPERIMENTAL SETUP.

Beat-to-beat SAI-PAI estimates were derived from the double blockade data set using Kalman filtering, whereas, in all of the other data sets, instantaneous SAI-PAI estimates with a 5-ms temporal resolution were calculated using the point-process modeling. Full methodological details can be found in the APPENDIX.

To allow the reader to reproduce the methodology, in the following section, generic Ψ values gathered from a multiple linear regression are reported using data from all of the available data/subjects undergoing autonomic blockade.

Working model coefficients Ψ_S and Ψ_P. Following are generalized values of sympathetic kernels Ψ_S gathered from multiple linear regression performed on data from all of the available data/subjects undergoing autonomic blockade (i.e., parasympathetic suppression), as well as parasympathetic kernels Ψ_P gathered from multiple linear regression performed on data from all of the available data/subjects undergoing autonomic blockade (i.e., sympathetic suppression).

The use of these coefficients, although with limited generality, is the first working attempt to estimate sympathetic and parasympathetic dynamics from ECG without the need of any calibration procedure at a single-subject level.

Particularly, results reported in the following sections were obtained using the following realizations of Ψ_S and Ψ_P coefficients: $\Psi_S = \{39.2343,\ 10.1963,\ -5.9242\}$ and $\Psi_P = \{28.4875,\ -17.3627,\ 5.8798,\ 12.0628,\ 5.6408,\ -7.0664,\ -5.6779,\ -3.9474\}$.

Considering also the standard deviation among realizations of Ψ_S and Ψ_P coefficients, statistical inference on healthy subjects is reported here (95% *t*-Student-based confidence interval). See Table 1.

Validation 1: tilt-table protocols. A first extensive validation was performed using data gathered from the tilt-table protocol, including stand-up, slow-tilting, and fast-tilting maneuvers. Instantaneous estimates of all of the features were obtained using the point-process modeling with Laguerre expansion (7, 53). To this extent, all KS plots and >98% of the autocorrelation samples fell within 95% confidence intervals, indicating that our modeling always provides a good characterization of the RR series, thus predicting heartbeats with satisfactory accuracy. Overall, KS distances were as low as 0.0220 ± 0.0056 (median $\pm$ MAD). Results from a comprehensive goodness-of-fit analysis are reported in the APPENDIX.

Instantaneous estimates from a single subject are reported in Fig. 2. From this exemplary visual comparison between LF vs. SAI, HF vs. PAI, and LF/HF vs. SAI/PAI, it is of striking evidence how responses from the gravitational changes are clearly tracked at the individual level by the new indexes (note the pattern corresponding to the vertical lines, indicating the postural transitions for SAI, PAI, and SAI/PAI). Importantly, the old frequency band quantification has been effective at the group level, but (as clear from the figure) has never been able to work at the individual level. Results from other subjects confirm this example, and a few more examples are reported in the APPENDIX. Instantaneous series averaged among all subjects are shown in Figs. 3, 4, and 5 aligned for each gravitational change: fast-tilt, slow-tilt, and stand-up, respectively. Several other instantaneous estimates at a single subject level are reported in the APPENDIX for further validation. Results give evidence that the proposed SAI and PAI measures, as well as the SAI/PAI outperform the traditional autonomic characterization given by standard HRV instantaneous spectral analysis (7). From the figures, it is possible to visually appreciate how the response from the proposed SAI, different from the LF power, increases after gravitational stress (with a further delay after slow tilt) and remains at higher levels than the baseline session, thus reflecting sustained sympathetic activation. Conversely, the LF sharply increases with stimulation after fast tilt (Fig. 3), behaves erratically with stand up (Fig. 5), and even decreases after slow-tilt (Fig. 4), possibly mirroring vascular-related blood pressure dynamic responses. Note the sharper step responses tracked by the PAI index compared with the HF measure.

Overall, we performed a comprehensive comparison of autonomic measures on the stand-up, slow-tilt, and fast-tilt transitions, including standard estimates defined in the time and frequency domains from a traditional linear AR model; instantaneous standard estimates defined in the time and frequency domains from a traditional linear AR point-process model (AR_{PP}) (7); instantaneous standard estimates defined in the time and frequency domains from a linear AR point-process model using the Laguerre expansion (ARL_{PP}) (53); and instantaneous SAI and PAI estimates from a point-process model having the kernels, Ψ_S and Ψ_P, calculated through:

- NEW (0): a multiple linear regression using subject-specific (i.e., performed for each subject) recording from one rest-upright condition.
- NEW (1): a multiple linear regression using subject-specific (i.e., performed for each subject) recording averaging Ψ_S and Ψ_P estimates from stand-up, slow-tilting, and fast-tilting conditions.
- NEW (2): a multiple linear regression using general values (i.e., calculated over all of the subjects), averaging Ψ_S and Ψ_P estimates from stand-up, slow-tilting, and fast-tilting conditions, following a leave-one-subject-out procedure.
- NEW (3): a multiple linear regression using general values (i.e., calculated over all of the subjects), averaging Ψ_S and Ψ_P estimates from the rest-tilt control session of an independent data set.
- NEW (4): a multiple linear regression using general values (i.e., calculated over all of the subjects), averaging Ψ_S and Ψ_P from subjects of an independent data set undergoing autonomic blockade (parasympathetic suppression $\rightarrow$ sympathetic kernels Ψ_S; sympathetic suppression $\rightarrow$ parasympa-

Table 1. *Confidence interval of sympathetic and parasympathetic coefficients Ψ*

	$j = 0$	$j = 1$	$j = 2$	$j = 3$	$j = 4$	$j = 5$	$j = 6$	$j = 7$
Ψ_{S_j}	39.2343 ± 16.9821	10.1963 ± 9.9895	−5.9242 ± 6.0936					
Ψ_{P_j}	28.4875 ± 11.4879	−17.3627 ± 8.4911	5.8798 ± 7.9916	12.0628 ± 7.2923	5.6408 ± 6.7928	−7.0664 ± 4.8948	−5.6779 ± 5.1945	−3.9474 ± 5.8938

Values are median absolute deviation ± SE. Ψ_{S_j}, sympathetic coefficient; Ψ_{P_j} parasympathetic coefficient.

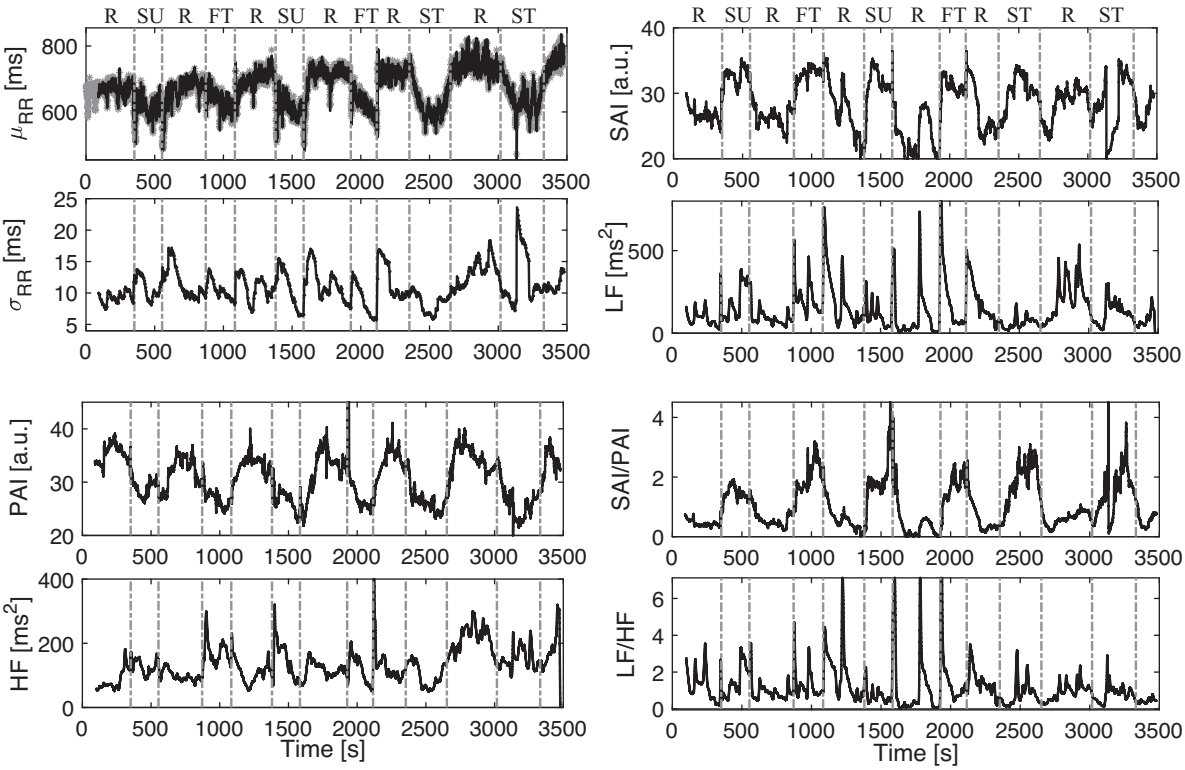

Fig. 2. Instantaneous heartbeat statistics computed from an exemplary subject of the tilt-table protocol. *Top left*: the estimated mean R-R interval at time t, $\mu_{RR}(t)$, superimposed on the recorded R-R series, and the instantaneous heartbeat standard deviation of the R-R intervals at time t, $\sigma_{RR}(t)$, are shown. Instantaneous sympathetic and parasympathetic activity, and sympathovagal balance as estimated through sympathetic activity index (SAI) and parasympathetic activity index (PAI), and ratio of SAI to PAI (SAI/PAI) measures, along with the low frequency (LF), high frequency (HF), and ratio of LF to HF (LF/HF) are shown in the other panels. Vertical dashed lines indicate the beginning and end of each experimental transition. For this subject, the first transition is from rest (R) to stand-up (SU) and back, the second is from R to fast tilt (FT) and back, the third from R to SU, then R to FT, and the final two are from R to slow tilt (ST) and back. Transitions are randomized for each subject. a.u., Arbitrary units.

thetic kernels Ψ_P. See *Derivation of the Novel Sympathetic and Parasympathetic Activity Measures* for details.)

Standard HRV measures, i.e., RMSSD (root mean square of the successive differences), pNN50 (the proportion derived by dividing the number of interval differences of successive NN intervals >50 ms by the total number of NN intervals) (%), HRV triangular index (HRV_tri_ind), and TINN (triangular interpolation of NN interval histogram), are also calculated and reported.

Numerical results using the NEW (4) estimation method are shown in Tables 2, 3, and 4. All other results are included in the APPENDIX.

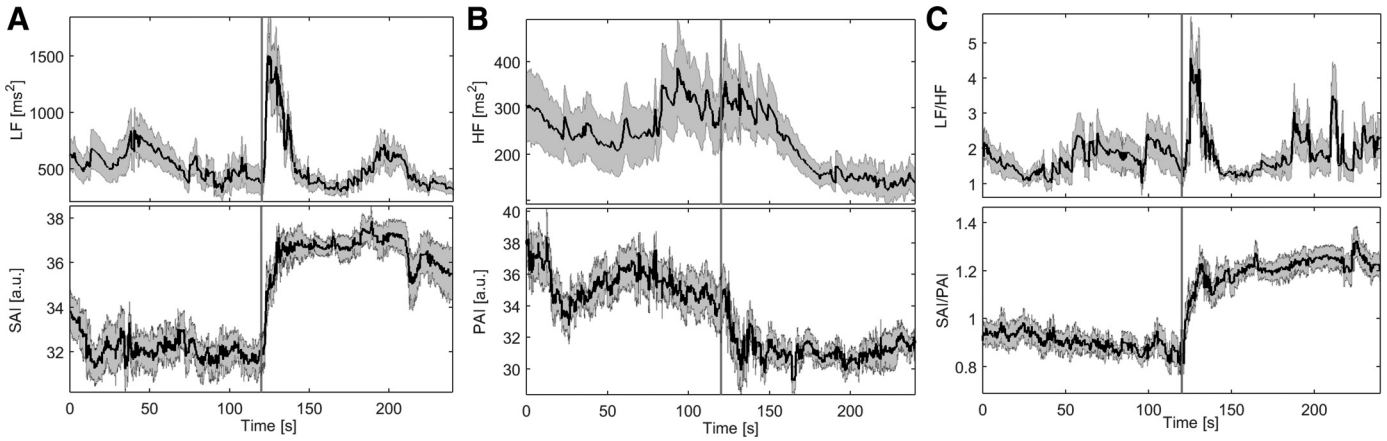

Fig. 3. Tilt-table protocol: fast-tilt. Instantaneous point-process estimates averaged along all subjects, aligned with the transitions before and after fast-tilt. *A*: estimated instantaneous power low frequency at time t, LF(t), and the sympathetic activity index at time t, SAI(t), can be compared. At each time, the median value is superimposed (solid line) on the standard error of the median (shaded area). Vertical line indicates the beginning of the fast-tilt maneuver. *B*: likewise, the estimated instantaneous power high frequency at time t, HF(t), and the parasympathetic activity index at time t, PAI(t), are shown. *C*: the estimated instantaneous LF-to-HF ratio at time t, LF/HF(t), and the SAI-to-PAI ratio at time t, SAI/PAI(t), can be compared. a.u., Arbitrary units.

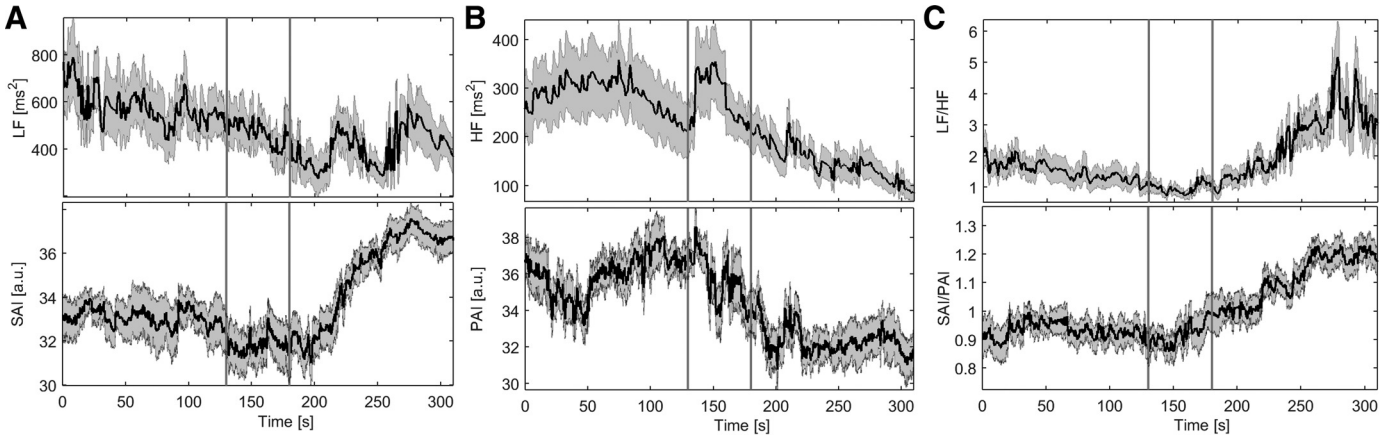

Fig. 4. Tilt-table protocol: slow-tilt. Instantaneous point-process estimates averaged along all subjects, aligned with the slow-tilt transitions. *A*: estimated instantaneous power low frequency at time t, LF(t), and the sympathetic activity index at time t, SAI(t), can be compared. At each time, the median value is superimposed (solid line) on the standard error of the median (shaded area). The two vertical lines indicate the start and end of the slow tilting maneuver. *B*: likewise, the estimated instantaneous power high frequency at time t, HF(t), and the parasympathetic activity index at time t, PAI(t), can be compared. *C*: the estimated instantaneous LF-to-HF ratio at time t, LF/HF (t), and the SAI-to-PAI ratio at time t, SAI/PAI(t), can be compared. a.u., Arbitrary units.

Concerning sympathetic activity, results show that SAI estimates are always able to effectively discern between resting and upright conditions. Using Ψ_S and Ψ_P kernels of general applicability, increased sympathetic activity after stand-up is significantly revealed, with $P < 4 \times 10^{-5}$, as well as after slow tilt ($P < 0.007$) and fast tilt ($P < 9 \times 10^{-4}$). No significant results are reported using indexes of LF power ($P > 0.05$). Likewise, for parasympathetic activity, results show that PAI estimates are always able to effectively discern between resting and upright conditions. Using Ψ_S and Ψ_P kernels of general applicability, decreased parasympathetic activity after stand-up was revealed with $P < 6 \times 10^{-4}$, as well as after slow tilt ($P < 0.011$) and fast tilt ($P < 0.002$). Significant results are achieved using indexes of HF power, as estimated through standard AR modeling on the slow tilt ($P < 0.03$). Statistical analysis for all other indexes yielded no significant results ($P > 0.05$). Finally, groupwise statistics of sympathovagal balance show that SAI/PAI estimates were always able to effectively discern between resting and upright conditions. Using Ψ_S and Ψ_P kernels of general applicability, increased sympathovagal balance after stand-up was revealed with $P < 4 \times 10^{-6}$, as well as after slow tilt ($P < 0.001$) and fast tilt ($P < 2.629 \times 10^{-4}$). No significant results were achieved using indexes of LF/HF ($P > 0.05$).

Validation 2: lower body negative pressure. A second validation of our SAI-PAI estimates was performed using data gathered from the LBNP protocol. Instantaneous estimates of all of the features were obtained using point-process modeling with Laguerre expansion (7, 53). All KS plots but three, and >98% of the autocorrelation samples fell within 95% confidence intervals, indicating a very good fit. Considering all of the 108 recordings, KS distances were as low as 0.0366 ± 0.0082 (median $\pm$ MAD). Results from a comprehensive goodness-of-fit analysis are reported in the APPENDIX. Instantaneous series averaged among all 58 subjects are shown in Fig. 6. Results of the statistical comparison are reported in Table 5. From the Fig. 6, it is possible to visually appreciate how the proposed SAI, different from the LF power, increases after gravitational stress by tracking a clear exponential-like step

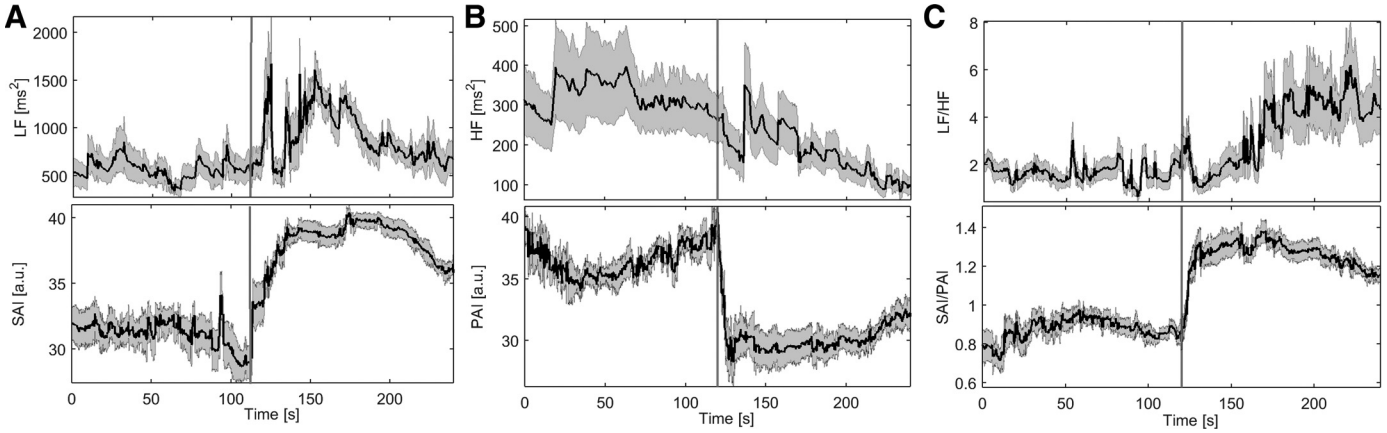

Fig. 5. Tilt-table protocol: stand up. Instantaneous point-process estimates averaged along all subjects, aligned with the stand-up transitions. *A*: the estimated instantaneous power low frequency at time t, LF(t), and the sympathetic activity index at time t, SAI(t), can be compared. At each time, the median value is superimposed (solid line) on the standard error of the median (shaded area). Vertical lines indicate the beginning of the stand-up maneuver. *B*: likewise, the estimated instantaneous power high frequency at time t, HF(t), and the parasympathetic activity index at time t, PAI(t), can be compared. *C*: the estimated instantaneous LF-to-HF ratio at time t, LF/HF (t), and the SAI-to-PAI ratio at time t, SAI/PAI(t), can be compared. a.u., Arbitrary units.

Table 2. *Results from the rest-stand-up experimental data set*

	Autonomic Index	Rest	Stand Up	*P* Value
Sympathetic activity	LF	516.16 ± 311.31	152.33 ± 379.46	0.270000
	SAI	30.03 ± 3.17	39.05 ± 2.05	0.000031
Parasympathetic activity	HF	337.17 ± 247.07	155.23 ± 73.60	0.408000
	PAI	35.91 ± 1.84	29.63 ± 3.25	0.000570
Sympathovagal balance	LF/HF	1.88 ± 1.36	3.25 ± 2.59	0.242000
	SAI/PAI	0.85 ± 0.14	1.29 ± 0.13	0.000003

Values are median absolute deviation ± SE. *P* values are obtained from the rank-sum test between the rest and stand-up sessions. HF, high frequency; LF, low frequency; LF/HF, ratio of LF to HF; PAI, parasympathetic activity index; SAI, sympathetic activity index; SAI/PAI, ratio of SAI to PAI.

response, thus reflecting sustained sympathetic activation. Conversely, the LF sharply increases with stimulation right after the step pressure change and then behaves erratically along time. Also here, note the sharper step responses tracked by the PAI index compared with the HF measure.

It should be noted that, based on the *P* values for this paradigmatic case, the proposed SAI and PAI measures, as well as the SAI/PAI, outperform the traditional autonomic characterization given by standard HRV instantaneous spectral analysis (7). Once again, the increase of sympathetic activity, as identified by the SAI index, presents a slower time constant than the parasympathetic one, which is identified by the PAI index.

Concerning sympathetic activity, results show that SAI estimates are able to effectively identify expected increases during LBNP conditions with respect to resting state with $P < 5 \times 10^{-16}$, despite that no significant statistics were obtained through indexes of LF power ($P > 0.05$).

Moreover, expected decreases in parasympathetic activity during LBNP are effectively revealed through PAI estimates with $P < 2 \times 10^{-12}$, as well as indexes of HF power ($P < 10^{-8}$), whereas increases in the sympathovagal balance during LBNP are identified through SAI/PAI estimates with $P < 8 \times 10^{-16}$, as well as indexes of LF/HF ($P < 2 \times 10^{-8}$).

Validation 3: handgrip. A further validation of our SAI-PAI estimates was performed using data gathered from the handgrip protocol. Instantaneous estimates of all of the features were obtained using point-process modeling with Laguerre expansion (7, 53). All KS plots but seven, and >98% of the autocorrelation samples fell within 95% confidence intervals, indicating a very good fit. Considering all 108 recordings, KS distances were as low as 0.0647 ± 0.0102 (median ± MAD). Results from a comprehensive goodness-of-fit analysis are reported in the APPENDIX. Instantaneous series from all subjects are shown in Fig. 7. Results of the statistical comparison are reported in Table 6.

Once again, the proposed SAI and PAI measures, as well as the SAI/PAI, outperform the traditional autonomic characterization given by standard HRV instantaneous spectral analysis (7). The increase in sympathetic activity during the handgrip task, with respect to baseline, is effectively identified by the SAI index, both visually (Fig. 6) and with statistical significance ($P < 0.006$). No significant statistics are reported through indexes of LF power ($P > 0.05$).

Furthermore, decreases in parasympathetic activity during handgrip are effectively revealed through PAI estimates with $P < 0.002$, as well as indexes of HF power ($P < 0.009$), whereas increases in sympathovagal balance during handgrip are identified through SAI/PAI estimates exclusively, with $P < 9 \times 10^{-4}$. No significant statistics are obtained through LF/HF indexes ($P > 0.05$).

DISCUSSION AND CONCLUSIONS

Despite widespread use during the last two decades, HRV analyses based on frequency domain techniques have faced significant challenges in assessing cardiac autonomic activity (17, 19, 40). Several pharmacological studies have confirmed the intrinsic ambiguity of this approach, as HRV-related changes <0.15 Hz are mediated by both cardiac vagal and sympathetic nerves (9, 23, 24, 42). In addition, changes in the LF power of HRV often occur in response to arterial blood pressure fluctuations, which cause HR fluctuations through the baroreflex (2). A variety of sophisticated methodologies have been proposed to address these issues (10, 58, 59, 63, 64, 66, 67). However, their impact in cardiovascular research has been limited due to methodological (e.g., stationarity, the need of a broadband HR spectrum) or practical shortcomings (e.g., the need of multivariate autonomic recordings, such as ECG and respiration). The issues are even more challenging for clinical monitoring, where relatively rudimentary concepts and simple computational algorithms for HRV analysis have been used for clinical monitoring. Moreover, using HRV spectra, several commercially available mobile applications have not been able to provide precise, reliable assessments of stress levels, sleep quality, or recovery from athletic activity (49, 60). These shortcomings in current autonomic measures are due, in part, to high

Table 3. *Results from the rest-slow tilt-table experimental data set*

	Autonomic Index	Rest	Titl-Table Slow	*P* Value
Sympathetic activity	LF	552.42 ± 388.69	368.13 ± 220.38	0.715000
	SAI	33.50 ± 3.17	36.05 ± 1.59	0.007000
Parasympathetic activity	HF	295.12 ± 192.60	128.92 ± 77.27	0.060000
	PAI	36.42 ± 2.92	31.96 ± 3.15	0.011000
Sympathovagal balance	LF/HF	1.39 ± 1.071	3.00 ± 1.43	0.126000
	SAI/PAI	0.95 ± 0.13	1.15 ± 0.13	0.001000

Values are median absolute deviation ± SE. *P* values are obtained from the rank-sum test between the rest and slow-tilt sessions. HF, high frequency; LF, low frequency; LF/HF, ratio of LF to HF; PAI, parasympathetic activity index; SAI, sympathetic activity index; SAI/PAI, ratio of SAI to PAI.

Table 4. *Results from the rest-fast tilt-table experimental data set*

	Autonomic Index	Rest	Titl-Table Fast	*P* Value
Sympathetic activity	LF	568.28 ± 299.64	504.37 ± 269.77	0.704000
	SAI	31.80 ± 2.21	36.79 ± 1.85	0.000870
Parasympathetic activity	HF	239.12 ± 177.12	203.04 ± 102.98	0.815000
	PAI	35.89 ± 2.95	30.62 ± 1.58	0.002000
Sympathovagal balance	LF/HF	1.82 ± 1.43	1.56 ± 0.65	0.977000
	SAI/PAI	0.87 ± 0.13	1.21 ± 0.13	0.000263

Values are median absolute deviation ± SE. *P* values are obtained from the rank-sum test between the rest and fast-tilt sessions. HF, high frequency; LF, low frequency; LF/HF, ratio of LF to HF; PAI, parasympathetic activity index; SAI, sympathetic activity index; SAI/PAI, ratio of SAI to PAI.

interindividual variability. Current techniques have not been accurate enough to provide meaningful autonomic measures that are valid for group analysis, while simultaneously being tailored to the individual subject, particularly for sympathetic activity.

This paper introduces a set of autonomic measures that differ from those used previously. PAI and SAI *1*) provide independent parasympathetic and sympathetic dynamics, *2*) exclusively use heartbeat intervals, *3*) can be computed continuously in real time without concerns of stationarity, and *4*) appear to be reliable for both group and individual assessment. The novel identification procedure is a simple nontrivial way to calculate noninvasive, time-resolved autonomic markers that have features of effectiveness, reliability, and high resolution in time. Importantly, the metrics offer the potential to continuously track cardiac autonomic control in both clinical and research settings. The methodology is also applicable to any sequence of heartbeat events, e.g., ECG, echocardiographic parameters, arterial pressure parameters, video signals, ballistogram, ultrawideband cardiogram, etc. The time-varying estimates of SAI and PAI were shown to provide instantaneous features consistent with a wide range of individual subject's conditions in a variety of autonomic states. Several estimation techniques can be used to obtain beat-to-beat or finite estimates in time using, e.g., Kalman or least squares methods, respectively. In addition, instantaneous SAI and PAI estimates can be obtained through point-process modeling (7, 53).

These novel measures were validated using data sets collected in controlled physiological conditions and involving well-known sympathovagal changes, including orthostatic changes from standing; slow tilting and fast tilting; autonomic blockade during postural changes; LBNP; and handgrip. In all of the cases evaluated, the results of the new technique demonstrated superiority at separating the sympathetic and parasympathetic components using the SAI and PAI signals, compared with existing methods.

By using comprehensive intersubject statistics computed every 5 ms, the SAI index correctly demonstrated the expected increases of sympathetic activation and vagal withdrawal in all of the autonomic scenarios that have been tested. The analyses are scientifically thorough, with time-varying estimates, avoiding the loss of information inherent in the static metrics typically reported in the literature. The results were also compared with three different reported methodologies: *1*) a simple window-based AR model demonstrating comparison to the published HRV guidelines (35); 2) a time-varying point-process AR model providing a comparison which accounts for nonstationary (7), and 3) a time-varying point-process model using Laguerre functions (53). For assessment of sympathetic and parasympathetic activity, SAI, PAI, and SAI/PAI appear to track expected physiological responses much more closely than LF, HF or LF/HF in all the data sets evaluated. The new parameters showed particular improvement in inter-subject variability, reflected in lower standard errors, and more significant difference in the statistical comparisons (see details in Tables A2, A3, and A4).

Importantly, the SAI and PAI measures are derived in a nonobvious and original way. Although the methodological framework may share relevant features adopted in the past, such as the use of Laguerre expansion (5), the derivation is the first attempt at proposing a proper combination of coefficients derived by Laguerre functions, which yield very specific fea-

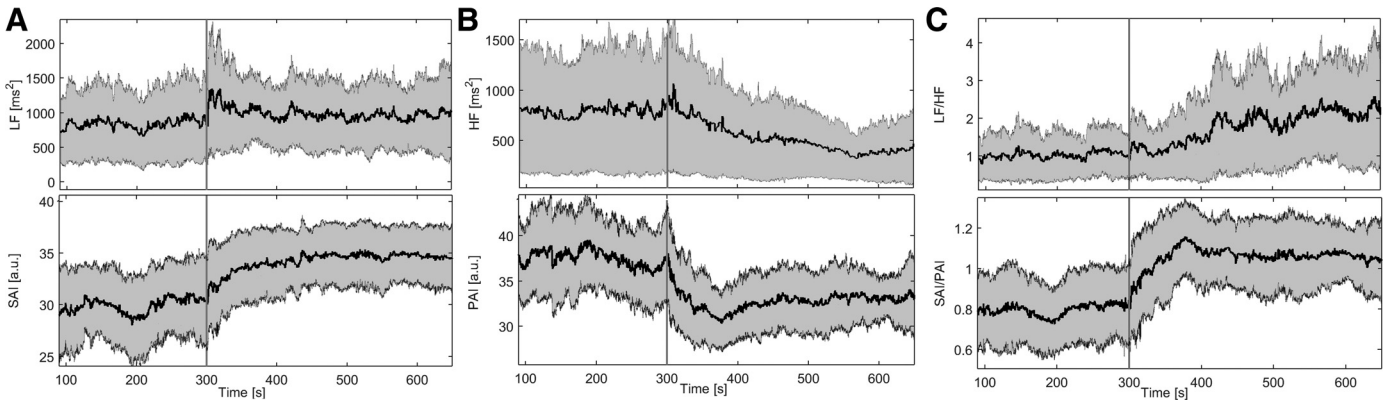

Fig. 6. Lower body negative pressure (LBNP) protocol. Instantaneous point-process estimates averaged along all subjects, aligned with the LBNP transitions. *A*: the estimated instantaneous power low frequency at time t, LF(t), and the sympathetic activity index at time t, SAI(t), are shown. At each time, the median value is superimposed (solid line) on the standard error of the median (shaded area). Vertical line indicates the beginning of the LBNP maneuver. *B*: likewise, the estimated instantaneous power high frequency at time t, HF(t), and the parasympathetic activity index at time t, PAI(t), are shown. *C*: the estimated instantaneous LF-to-HF ratio at time t, LF/HF (t), and the SAI-to-PAI ratio at time t, SAI/PAI(t) are shown. a.u., Arbitrary units.

Table 5. *Comparison of autonomic indexes between rest and LBNP*

Autonomic Index	Rest	LBNP	*P* Value
LF, ms^2	875.530 ± 525.734	964.204 ± 402.282	0.440
SAI, AU	29.890 ± 3.828	34.353 ± 2.708	3.950×10^{-16}*
HF, ms^2	766.415 ± 602.566	457.434 ± 324.865	9.248×10^{-8}*
PAI, AU	38.218 ± 3.586	32.647 ± 2.712	1.665×10^{-12}*
LF/HF	1.043 ± 0.578	1.542 ± 0.878	1.614×10^{-8}*
SAI/PAI	0.774 ± 0.146	1.067 ± 0.151	7.496×10^{-16}*

Values are median absolute deviation ± SE. *P* values are from the sign-rank nonparametric test for paired data. AU, arbitrary units; HF, high frequency; LF, low frequency; LF/HF, ratio of LF to HF; LBNP, lower body negative pressure; PAI, parasympathetic activity index; SAI, sympathetic activity index; SAI/PAI, ratio of SAI to PAI. *Significant differences between rest and LBNP sessions.

tures in the time and frequency domains (31, 33, 53). It is also noteworthy that, once a standard AR model has been identified along the Laguerre bases (i.e., after convolving the original R-R interval series with the Laguerre bases), the use of SAI and PAI measures does not need calibration. The derivation of preestimated kernels of general applicability for the SAI and PAI estimation are taken from data gathered from selective sympathetic and parasympathetic blockade.

The overall approach stems from the intuitive hypothesis that the cholinergic and adrenergic systems have different temporal dynamics that overlap in the frequency domain. Thus a proper weighted sum and/or subtraction of primitives derived from orthonormal Laguerre bases is able to reflect the actual autonomic activity, disentangling the specific sympathetic and parasympathetic contributions. In the frequency domain, for a given α, the spectra of Laguerre functions have equal magnitude and different phase spectra. The classic HRV analysis is limited by the predefined frequency ranges (VLF, LF, and HF), whereas the Laguerre functions do not define a space in the frequency domain but constitute a set of mathematical functions, characterizing a specific fine modulation of the number of oscillations across zero, as well as very specific time responses.

An important limitation of the study is that the identification of kernels of general applicability has been performed using data coming from a limited number of subjects. Consequently, nonparametric paired comparisons using data from selective parasympathetic and sympathetic blockade resulted in nonsignificant *P* values; however, central trends were as expected. Although an extensive validation was performed of the proposed SAI and PAI through more than 230 ECG recordings, all of the data were from healthy volunteers. Therefore, it cannot be excluded that a more accurate identification of Ψ_S and Ψ_P kernels of general applicability may be necessary when dealing with data from subjects with various cardiovascular pathologies or subjects with peculiar heartbeat dynamics (e.g., infants and newborns). Likewise, it cannot be excluded that the Ψ_S and Ψ_P kernel estimation could be improved by considering cases where subjects elicit peculiar respiratory patterns. Also, the absolute value of SAI and PAI estimates is currently dependent on the arbitrary ranges chosen for the fitting procedure described in *Derivation of the Novel Sympathetic and Parasympathetic Activity Measures* above. A proper study on the scalability of SAI and PAI estimates should be performed to obtain normalized indexes with improved interpretability. Finally, depending on the estimation method used to identify the Laguerre coefficients, the initial part of the recording is left without actual SAI and PAI estimates because the point-process modeling needs at least the first 70 s of ECG, which must be used for model initialization (7, 53). There is also likely room to improve the proposed identification using data from a more diverse pool of subjects undergoing selective autonomic blockade while undergoing significant orthostatic changes. Moreover, given the ability of our model to characterize the probabilistic structure of R-R interval generation as related to mean HR, future studies might consider more detailed analyses on the relationship between these two variables

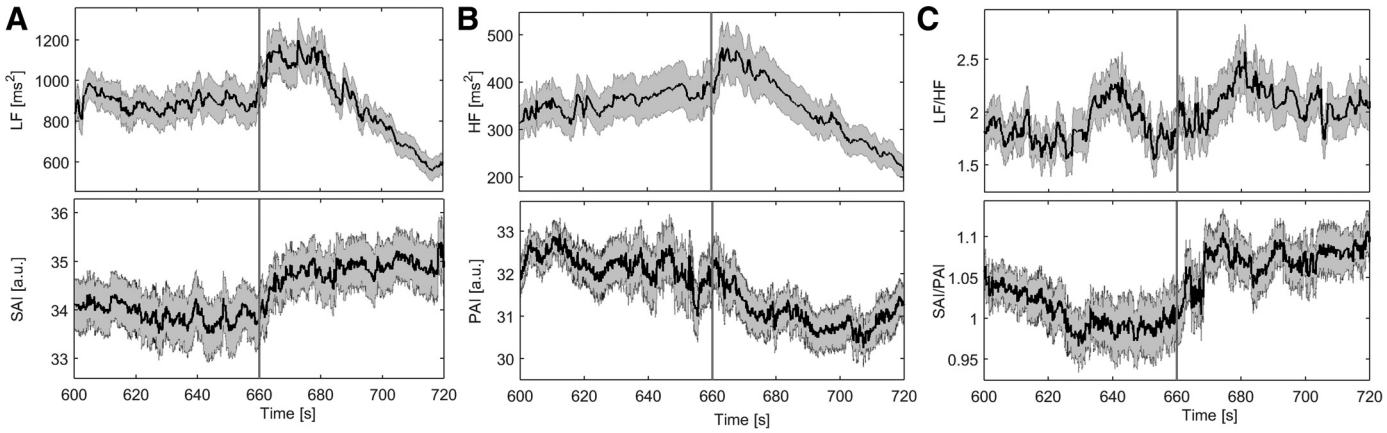

Fig. 7. Handgrip protocol. Instantaneous point-process estimates averaged along all subjects, aligned with the handgrip transitions. *A*: the estimated instantaneous power low frequency at time *t*, LF(*t*), and the sympathetic activity index at time *t*, SAI(*t*), are shown. At each time, the median value is superimposed (solid line) on the standard error of the median (shaded area). Vertical line indicates the beginning of the handgrip task. *B*: likewise, the estimated instantaneous power high frequency at time *t*, HF(*t*), and the parasympathetic activity index at time *t*, PAI(*t*), are shown. *C*: the estimated instantaneous LF-to-HF ratio at time *t*, LF/HF (*t*), and the SAI-to-PAI ratio at time *t*, SAI/PAI(*t*) are shown. a.u., Arbitrary units.

Table 6. *Comparison of autonomic indexes between baseline and handgrip*

Autonomic Index	Baseline	Handgrip	*P* Value
LF, ms^2	982.257 ± 579.178	924.135 ± 479.580	0.135
SAI, AU	34.569 ± 2.946	35.719 ± 3.022	0.006*
HF, ms^2	414.418 ± 324.917	416.781 ± 332.342	0.009*
PAI, AU	33.055 ± 2.979	31.527 ± 2.744	0.002*
LF/HF	2.059 ± 1.438	2.465 ± 1.636	0.302
SAI/PAI	1.052 ± 0.179	1.130 ± 0.153	8.584×10^{-4}*

Values are median absolute deviation ± SE. *P* values are from the sign-rank nonparametric test for paired data. AU, arbitrary units; HF, high frequency; LF, low frequency; LF/HF, ratio of LF to HF; LBNP, lower body negative pressure; PAI, parasympathetic activity index; SAI, sympathetic activity index; SAI/PAI, ratio of SAI to PAI. *Significant differences between rest and LBNP sessions.

as linked to other cardiovascular correlates (e.g., respiration, blood pressure, etc.). Future studies might include a variety of different manipulations of cardiovascular control.

Despite the above limitations, the strength of the algorithm lies in estimating SAI-PAI values through an appropriate combination of orthonormal Laguerre bases. When applied to physiological data, there has been strong statistical support for demonstrating changes in sympathovagal balance in all of the experimental settings. Note that the proposed framework has been particularly successful in significantly reducing intersubject variability with respect to HRV frequency domain analysis. These improvements enhance the statistical power of the SAI and PAI measures compared with standard measures using LF and HF powers (in some instances by as much as 10^{16}).

By definition, SAI and PAI are dimensionless numbers. Moreover, SAI and PAI estimates are relative to "reference levels" of sympathetic and parasympathetic activity during supine resting state, and upright position after postural change. By definition, the actual value of such "reference levels" is arbitrary, as long as prior constraints from physiological dynamics are taken into account (dominant parasympathetic activity during supine resting state, dominant sympathetic activity during upright position after postural change).

From a methodological point of view, extension of the SAI-PAI derivation with nonlinear modeling could open new avenues for the estimation of sympathetic and parasympathetic nonlinear dynamics, as well as effective quantification of nonlinear sympathetic-parasympathetic interactions, which may be based on bispectral and other higher order spectral analyses. There are a variety of major clinical and nonclinical applications using SAI-PAI estimates. Finally, since the SAI and PAI measures are derived from heartbeats exclusively, so it is possible to calculate them through any portable, possibly wearable device carrying heartbeat event information.

APPENDIX

Autoregressive Models and Laguerre Expansion

Let us consider a general formulation of an AR model:

$$y(k) = \mathbf{F}\big[y(k-1), y(k-2), ..., y(k-M)\big] + \epsilon(k) \qquad (A1)$$

By taking into account a linear combination of the past events, the AR model can be can be written as following:

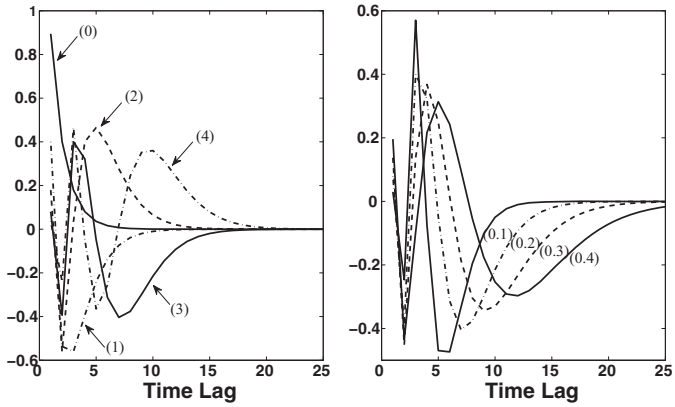

Fig. A1. *Left*: First four Laguerre functions for $\alpha = 0.2$ plotted over the first 25 lags. The order of each Laguerre basis is indicated in parentheses. *Right*: the third Laguerre functions for $\alpha = 0.1$, 0.2, 0.3, and 0.4. The corresponding α value is indicated in parentheses.

$$y(k) = \gamma_0 + \sum_{i=1}^{M} \gamma_1(i) y(k-i) + \epsilon(k) \qquad (A2)$$

where $\epsilon(k)$ are independent, identically distributed Gaussian random variables, and M is the memory of the model. Due to the AR structure of *Eq. A2*, the system can be identified with only exact knowledge of the output data and with only few assumptions on the input data. To improve the system identification process (i.e., γ_0, γ_1 estimations) and to reduce the number of required parameters, it is possible to expand the AR kernels by means of orthonormal bases. A widely used expansion uses the Laguerre functions (31, 33, 53). Specifically, let us define the *j*th-order discrete time orthonormal Laguerre function (see Fig. A1):

$$\phi_j(k) = \alpha^{\frac{k-j}{2}}(1-\alpha)^{\frac{1}{2}} \sum_{i=0}^{j} (-1)^i \binom{k}{i} \binom{j}{i} \alpha^{j-i}(1-\alpha)^i, (k \geq 0)$$

where α is the discrete-time Laguerre parameter ($0 < \alpha < 1$), which determines the rate of exponential asymptotic decline of these functions.

Given the Laguerre function, $\phi_j(k)$, and the signal, $y(k)$, the *j*th-order Laguerre filter output is:

$$l_j(k) = \sum_{i=0}^{\infty} \phi_j(i) y(k-i-1) \qquad (A3)$$

The computation of the Laguerre filter output can be accelerated significantly by use of the following recursive relation (31, 33, 53):

$$l_0(k) = \sqrt{\alpha} l_0(k-1) + \sqrt{1-\alpha} y(k-1) \qquad (A4)$$

$$l_j(k) = \sqrt{\alpha} l_j(k-1) + \sqrt{\alpha} l_{j-1}(k) + \qquad (A5)$$

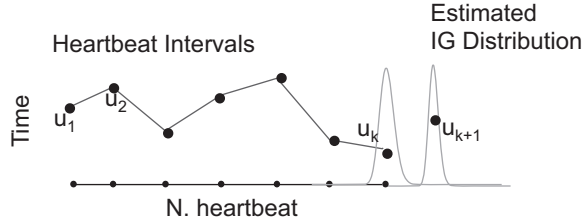

Fig. A2. Graphical representation of point-process modeling of heartbeat dynamics. The horizontal axis represents the counting process along the number (*N*) of heartbeats, whereas the vertical axis represents the duration of heartbeat intervals. Inverse-Gaussian (IG) distributions (*right*) characterize the prediction of the future heartbeat event along the time. u_1, u_2, u_k, and u_{k+1} indicate the times of heartbeat events. (From Ref. 55 with permission.)

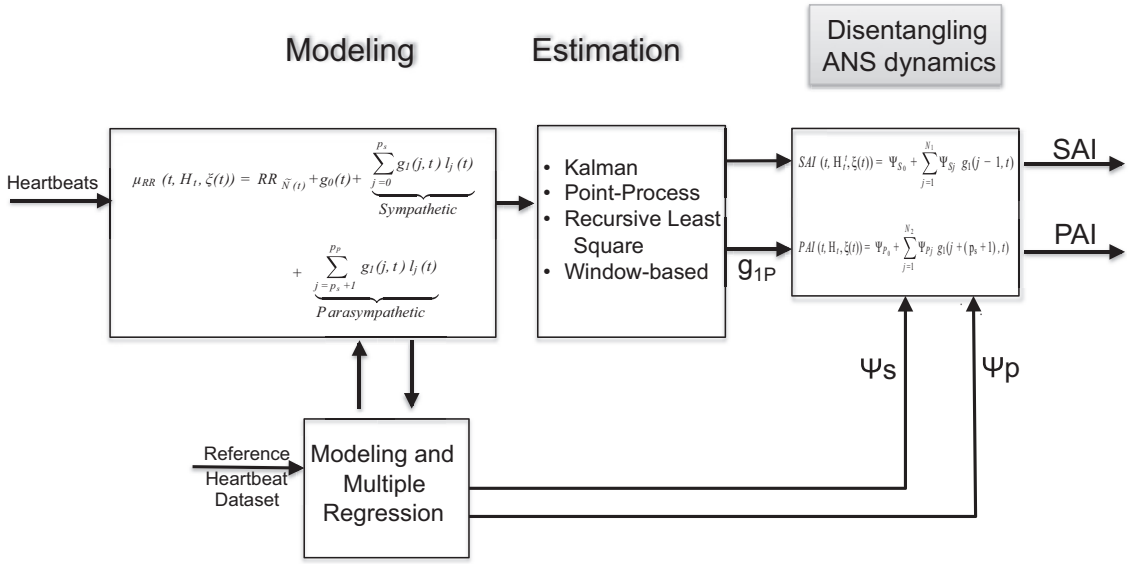

Fig. A3. Block scheme of the modeling and estimation stages involved in the sympathetic activity index (SAI)-parasympathetic activity index (PAI) calculation. ANS, autonomic nervous system; g_{1S}, g_1 sympathetic coefficient; g_{1P}, g_1 parasympathetic coefficient; Ψ_S, sympathetic coefficient; Ψ_P, parasympathetic coefficient.

$$\sqrt{\alpha} l_{j-1}(k-1),\ j \geq 1 \tag{A6}$$

Since the $\{\phi_i(t)\}$ form a complete orthonormal set in functional space $\mathcal{L}_2$, we can write (43):

$$\gamma_0 = g_0 \tag{A7}$$

$$\gamma_1(i) = \sum_{j=0}^{P} g_1(j)\phi_j(i) \tag{A8}$$

Here g_0 and $g_1(j)$ are constant coefficients. The expansion goes to zero as i goes to infinity. Using *Eqs. A3*, *A7*, and *A8*, the model in *Eq. A2* becomes:

$$y(k) = g_0 + \sum_{j=0}^{P} g_1(j) l_j(k) + \epsilon(k) \tag{A9}$$

hereinafter called AR with Laguerre expansion (ARL) model. The number of parameters to estimate is $N = 1 + (P + 1)$. Although the Laguerre filters have infinite memory, the AR model corresponding to the ARL representation can be truncated to an order M, which depends on how fast the Laguerre functions decade to zero. It is also noteworthy that, when $\alpha = 0$, the filter output becomes $l_j(k) = (-1)^j y(k - j - 1)$ and the ARL model corresponds to the AR model apart for the sign.

Time-Varying Implementation

The iterative estimation along time of the novel SAI-PAI measures can be performed using several signal processing methods. For example, a simple Kalman filtering can be used to track the SAI-PAI dynamics at each heartbeat, whereas an instantaneous estimation (i.e., at each moment in time) can be performed using the point-process modeling. Of note, traditional recursive least-squares and window-based methods can also be applied.

Heartbeat interval point-process model. A random point process is a stochastic process that can be thought of as registering the occurrence in time of discrete events (4). Point-process theory has been widely used in modeling various types of random events (e.g., eruptions of earthquakes, queueing of customers, spiking of neurons,

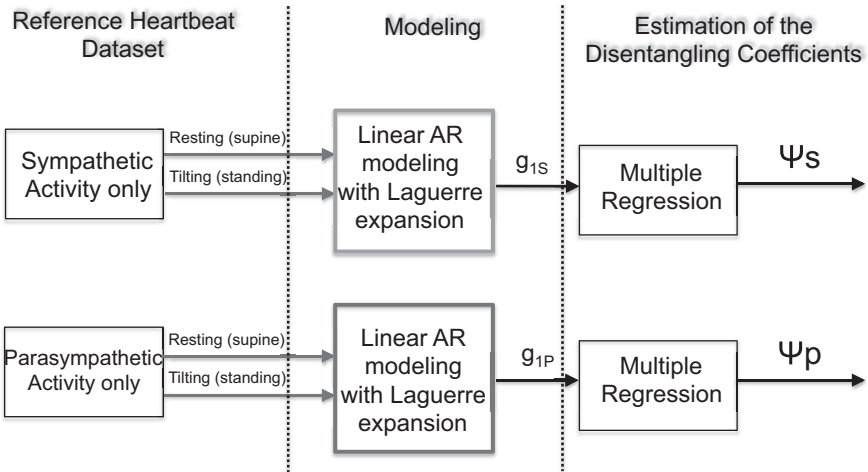

Fig. A4. Scheme detail of the "Model and Multiple Regression" block included in Fig. A3. g_{1S}, g_1 sympathetic coefficient; g_{1P}, g_1 parasympathetic coefficient; Ψ_S, sympathetic coefficient; Ψ_P, parasympathetic coefficient.

Table A1. *Comparison of autonomic indexes between baseline and handgrip*

	ACP-SSD			KS Distance		
Autonomic Index	Interval	Minimum	Maximum	Interval	Minimum	Maximum
Tilt-table	0.024 ± 0.0060	0.0042	0.0459	0.022 ± 0.0056	0.0078	0.0412
Lower body negative pressure	0.0891 ± 0.066	0.001	0.336	0.0366 ± 0.0082	0.0146	0.0797
Handgrip	0.0228 ± 0.0207	0.002	0.160	0.0647 ± 0.0102	0.0373	0.1091

Intervals are expressed as median ± median absolute deviation. ACP-SSD, autocorrelation plot-sum of the squared distances; KS, Kolmogorov-Smirnov.

etc.), where the timing of the events is of central interest. Bearing a similar spirit, the point-process theory has been used for modeling human heartbeats (7, 12, 51–54). The point-process framework primarily defines the probability of having a heartbeat event at each moment in time (see Fig. A2).

A parametric formulation of the probability function allows for a systematic, parsimonious estimation of the parameter vector in a recursive way and at any desired time resolution. Instantaneous indexes can then be derived from the parameters to quantify important features as related to cardiovascular control dynamics. Mathematically, let $(0,T]$ denote the observation interval and $0 \leq u_1 <\ldots< u_k < u_{k+1} <\ldots< u_K \leq T$ the times of the events. For $t \in (0,T]$, let $N(t) = \max\{k : u_k \leq t\}$ be the sample path of the associated counting process. Its differential, $dN(t)$, denotes a continuous-time indicator function, where $dN(t) = 1$, when there is an event (such as the ventricular contraction) or $dN(t) = 0$, otherwise. Let us define also a

Table A2. *Results from the rest-stand up experimental data set*

Statistical Index	Model	Rest	Stand Up	*P* Value
μ_{RR}, ms	AR_{PP}	906.17 ± 116.21	774.48 ± 80.41	0.015907
	ARL_{PP}	914.94 ± 122.70	773.46 ± 80.67	0.011924
	AR	910.94 ± 123.08	781.92 ± 55.96	0.013141
σ_{RR}, ms	AR_{PP}	19.69 ± 9.37	15.84 ± 5.06	0.406973
	ARL_{PP}	19.72 ± 9.37	16.57 ± 4.89	0.521672
	AR	47.48 ± 18.59	48.65 ± 16.42	0.998264
Sympathetic activity	LF(AR_{PP})	328.54 ± 260.34	410.03 ± 305.24	0.986259
	LF(ARL_{PP})	516.16 ± 311.31	152.33 ± 379.46	0.270000
	LF(AR)	349.86 ± 331.22	514.13 ± 506.35	0.947366
	$SAI_{NEW(0)}$	8.78 ± 1.21	12.55 ± 0.87	0.000078
	$SAI_{NEW(1)}$	8.52 ± 2.08	12.83 ± 0.34	0.000155
	$SAI_{NEW(2)}$	9.14 ± 0.87	10.11 ± 1.17	0.027497
	$SAI_{NEW(3)}$	33.05 ± 5.59	43.56 ± 5.15	0.000256
	$SAI_{NEW(4)}$	30.03 ± 3.17	39.05 ± 2.05	0.000031
Parasympathetic activity	HF(AR_{PP})	179.39 ± 149.43	76.13 ± 51.63	0.125312
	HF(ARL_{PP})	337.17 ± 247.07	155.23 ± 73.60	0.408000
	HF(AR)	234.17 ± 150.02	121.52 ± 71.68	0.088179
	$PAI_{NEW(0)}$	10.83 ± 1.01	7.16 ± 1.97	0.001805
	$PAI_{NEW(1)}$	11.37 ± 0.84	8.93 ± 1.56	0.028127
	$PAI_{NEW(2)}$	11.42 ± 1.09	10.00 ± 0.38	0.002437
	$PAI_{NEW(3)}$	38.39 ± 3.20	32.03 ± 3.74	0.002631
	$PAI_{NEW(4)}$	35.91 ± 1.84	29.63 ± 3.25	0.000570
Sympathovagal balance	LF/HF(AR_{PP})	1.37 ± 0.78	2.58 ± 2.41	0.221391
	LF/HF(ARL_{PP})	1.88 ± 1.36	3.25 ± 2.59	0.242000
	LF/HF(AR)	0.87 ± 0.66	0.89 ± 0.89	0.597419
	$SAI/PAI_{NEW(0)}$	0.86 ± 0.30	1.49 ± 0.17	0.002463
	$SAI/PAI_{NEW(1)}$	0.81 ± 0.19	1.35 ± 0.29	0.001088
	$SAI/PAI_{NEW(2)}$	0.80 ± 0.14	1.12 ± 0.11	0.000650
	$SAI/PAI_{NEW(3)}$	0.83 ± 0.18	1.38 ± 0.23	0.000014
	$SAI/PAI_{NEW(4)}$	0.85 ± 0.14	1.29 ± 0.13	0.000003
RMSSD, ms		26.28 ± 9.78	19.46 ± 4.41	0.144596
pNN50, %		5.98 ± 5.89	2.18 ± 2.18	0.098656
HRV_tri_ind		8.10 ± 1.71	7.61 ± 2.01	0.605398
TINN, ms		147.50 ± 40.00	185.00 ± 25.00	0.563922

Values are median absolute deviation ± SE. *P* values are obtained from the rank-sum test between the rest and stand-up sessions. AR, estimates from linear autoregressive model; AR_{PP}, estimates from linear point-process method; ARL_{PP}, estimates from linear point-process method with Laguerre expansion; HF, high frequency; HRV_tri_ind, HRV triangular index; LF, low frequency; LF/HF, ratio of LF to HF; NEW(0), a multiple linear regression using subject-specific (i.e., performed for each subject) recording from one rest-upright condition; NEW(1), a multiple linear regression using subject-specific (i.e., performed for each subject) recording averaging Ψ_S and Ψ_P estimates from stand-up, slow, and fast-tilting conditions; NEW(2), a multiple linear regression using general values (i.e., calculated over all of the subjects), averaging Ψ_S and Ψ_P estimates from stand-up, slow- and fast-tilting conditions, following a leave-one-subject-out procedure; NEW(3), a multiple linear regression using general values (i.e., calculated over all of the subjects) averaging Ψ_S and Ψ_P estimates from the rest-tilt control session of an independent data set; NEW(4), a multiple linear regression using general values (i.e., calculated over all of the subjects) averaging Ψ_S and Ψ_P from subjects of an independent data set undergoing autonomic blockade (parasympathetic suppression → sympathetic kernels Ψ_S; sympathetic suppression → parasympathetic kernels Ψ_P); PAI, parasympathetic activity index; pNN50, the proportion derived by dividing the number of interval differences of successive NN intervals >50 ms by the total number of NN intervals; RMSSD, root mean square of the successive differences; SAI, sympathetic activity index; SAI/PAI, ratio of SAI to PAI; TINN; triangular interpolation of NN interval histogram; μ_{RR}, estimated mean R-R interval; σ_{RR}, standard deviation of the R-R intervals.

left continuous function $\tilde{N}(t) = \lim_{\tau \to t^-} N(\tau) = \max\{k : u_k < t\}$, which will be useful in the following definitions.

By treating the R-waves as discrete events, we may develop a point-process probability model in the continuous time domain (7). Assuming history dependence, the probability density of the waiting time $t - u_j$ until the next R-wave event follows an inverse Gaussian model:

$$f\left[t|\mathcal{H}_t, \xi(t)\right] = \left[\frac{\xi_0(t)}{2\pi(t-u_j)^3}\right]^{\frac{1}{2}} \times \exp\left(-\frac{1}{2}\frac{\xi_0(t)\left\{t-u_j-\mu_{RR}\left[t,\mathcal{H}_t,\xi(t)\right]\right\}^2}{\mu_{RR}\left[t,\mathcal{H}_t,\xi(t)\right]^2(t-u_j)}\right) \quad (A10)$$

where $j = \tilde{N}(t)$ denotes the index of the previous R-wave event occurred before time t, $\mathcal{H}_t = (u_j, RR_j, RR_{j-1}, ..., RR_{j-M+1})$, $\xi(t)$ is the vector of the time-varing parameters, μ_{RR} $[t, \mathcal{H}_t, \xi(t)]$ represents the first-moment statistic (mean) of the distribution, and $\xi_0(t) = \theta > 0$ denotes the shape parameter of the inverse Gaussian distribution, (as $\theta/\mu \to \infty$, the inverse Gaussian distribution converges to a Gaussian distribution). The function f $[t \mid \mathcal{H}_t, \xi(t)]$ indicates the probability of having a beat at time t, given that a previous beat has occurred at u_j, and μ_{RR} $[t, \mathcal{H}_t, \xi(t)]$ can be interpreted as signifying the prediction of the time when the next beat is expected to occur. By definition, f $[t \mid \mathcal{H}_t, \xi(t)]$ is characterized at each moment in time, at the beat as well as in between beats.

The use of an inverse Gaussian distribution to characterize the R-R interval occurrences is motivated by the fact that, if the rise of the membrane potential to a threshold initiating the cardiac contraction is modeled as a Gaussian random walk with drift, then the probability density of the times between threshold crossings (the R-R intervals) is indeed the inverse Gaussian distribution (7). In Chen et al. (11), our laboratory has compared heartbeat interval fitting point process models using different probability distributions, and found that the inverse Gaussian model achieved the overall best fitting results. The parameter μ_{RR} $[t, \mathcal{H}_t, \xi(t)]$ denotes the instantaneous R-R mean that can be modeled as a generic function of the past (finite) R-R values $\mu_{RR}[t, \mathcal{H}_t, \xi(t)] = g[RR_{\tilde{N}(t)}, RR_{\tilde{N}(t)-1}, ..., RR_{\tilde{N}(t)-h+1}]$, where $RR_{\tilde{N}(t)-j+1}$

Table A3. *Results from the rest-slow tilt-table experimental data set*

Statistical Index	Model	Rest	Tilt-Table Slow	*P* Value
μ_{RR}, ms	AR_{PP}	875.25 ± 73.14	765.03 ± 58.91	0.000512
	ARL_{PP}	877.80 ± 72.50	764.79 ± 56.81	0.000412
	AR	879.59 ± 75.09	772.82 ± 46.10	0.001063
σ_{RR}, ms	AR_{PP}	21.51 ± 6.07	15.13 ± 4.95	0.057883
	ARL_{PP}	22.29 ± 5.92	15.11 ± 4.62	0.057883
	AR	52.57 ± 17.69	62.80 ± 16.30	0.843425
Sympathetic activity	LF(AR_{PP})	417.76 ± 240.68	332.88 ± 162.72	0.438254
	LF(ARL_{PP})	552.42 ± 388.69	368.13 ± 220.38	0.715000
	LF(AR)	465.03 ± 241.99	394.37 ± 310.24	0.661443
	$SAI_{NEW(0)}$	8.18 ± 1.50	11.14 ± 1.48	0.000965
	$SAI_{NEW(1)}$	9.22 ± 0.80	10.00 ± 1.16	0.052808
	$SAI_{NEW(2)}$	9.26 ± 0.56	10.52 ± 0.72	0.000970
	$SAI_{NEW(3)}$	30.78 ± 5.19	35.54 ± 5.45	0.011087
	$SAI_{NEW(4)}$	33.50 ± 3.17	36.05 ± 1.59	0.007000
Parasympathetic activity	HF(AR_{PP})	235.59 ± 166.53	88.15 ± 68.42	0.046554
	HF(ARL_{PP})	295.12 ± 192.60	128.92 ± 77.27	0.060000
	HF(AR)	263.67 ± 141.88	150.51 ± 74.30	0.050001
	$PAI_{NEW(0)}$	11.96 ± 2.00	7.27 ± 2.58	0.000177
	$PAI_{NEW(1)}$	14.09 ± 0.41	9.13 ± 2.40	0.001355
	$PAI_{NEW(2)}$	11.66 ± 0.93	10.25 ± 0.65	0.000708
	$PAI_{NEW(3)}$	39.14 ± 2.67	36.02 ± 1.01	0.066003
	$PAI_{NEW(4)}$	36.42 ± 2.92	31.96 ± 3.15	0.011000
Sympathovagal balance	LF/HF(AR_{PP})	1.03 ± 0.74	2.73 ± 1.64	0.209343
	LF/HF(ARL_{PP})	1.39 ± 1.071	3.00 ± 1.43	0.126000
	LF/HF(AR)	0.66 ± 0.23	1.21 ± 0.68	0.168735
	$SAI/PAI_{NEW(0)}$	0.66 ± 0.19	1.51 ± 0.69	0.000189
	$SAI/PAI_{NEW(1)}$	0.63 ± 0.09	1.18 ± 0.33	0.000376
	$SAI/PAI_{NEW(2)}$	0.82 ± 0.12	0.95 ± 0.07	0.004746
	$SAI/PAI_{NEW(3)}$	0.81 ± 0.20	1.05 ± 0.21	0.007233
	$SAI/PAI_{NEW(4)}$	0.95 ± 0.13	1.15 ± 0.13	0.001000
RMSSD, ms		32.10 ± 12.56	19.68 ± 4.52	(lt)0.05
pNN50, %		10.20 ± 9.47	1.74 ± 1.37	(lt)0.02
HRV_tri_ind		8.03 ± 1.41	7.31 ± 1.61	(mt)0.05
TINN, ms		195.00 ± 70.00	150.00 ± 45.00	(mt)0.05

Values are median absolute deviation ± SE. *P* values are obtained from the rank-sum test between the rest and slow-tilt sessions. AR, estimates from linear autoregressive model; AR_{PP}, estimates from linear point-process method; ARL_{PP}, estimates from linear point-process method with Laguerre expansion; HF, high frequency; HRV_tri_ind, HRV triangular index; LF, low frequency; LF/HF, ratio of LF to HF; NEW(0), a multiple linear regression using subject-specific (i.e., performed for each subject) recording from one rest-upright condition; NEW(1), a multiple linear regression using subject-specific (i.e., performed for each subject) recording averaging Ψ_S and Ψ_P estimates from stand-up, slow, and fast-tilting conditions; NEW(2), a multiple linear regression using general values (i.e., calculated over all of the subjects), averaging Ψ_S and Ψ_P estimates from stand-up, slow- and fast-tilting conditions, following a leave-one-subject-out procedure; NEW(3), a multiple linear regression using general values (i.e., calculated over all of the subjects) averaging Ψ_S and Ψ_P estimates from the rest-tilt control session of an independent data set; NEW(4), a multiple linear regression using general values (i.e., calculated over all of the subjects) averaging Ψ_S and Ψ_P from subjects of an independent data set undergoing autonomic blockade (parasympathetic suppression → sympathetic kernels Ψ_S; sympathetic suppression → parasympathetic kernels Ψ_P); PAI, parasympathetic activity index; pNN50, the proportion derived by dividing the number of interval differences of successive NN intervals >50 ms by the total number of NN intervals; RMSSD, root mean square of the successive differences; SAI, sympathetic activity index; SAI/PAI, ratio of SAI to PAI; TINN; triangular interpolation of NN interval histogram; μ_{RR}, estimated mean R-R interval; σ_{RR}, standard deviation of the R-R intervals.

denotes the previous *j*th R-R interval occurred before the present time *t*. In our laboratory's previous work (6, 11), the history dependence is defined by expressing the instantaneous mean μ_{RR} $[t, \mathcal{H}_t, \xi(t)]$ as a linear combination of present and past R-R intervals (in terms of an AR model), i.e., function *g* is linear.

Concerning the parameter estimation, we used a Newton-Raphson procedure to maximize the local log-likelihood and compute the local maximum-likelihood estimate of $\xi(t)$ (7, 53) within $W = 90$ *s*. Because there is significant overlap between adjacent local likelihood intervals, we started the Newton-Raphson procedure at *t* with the previous local maximum-likelihood estimate at time $t - \delta$, in which δ defines how much the local likelihood time interval is shifted to compute the next parameter update. The model goodness-of-fit is based on the KS test and associated KS statistics (see details in Refs. 7, 53). Autocorrelation plots were considered to test the independence of the model-transformed intervals (7, 53). Once the model order is determined, the initial model coefficients were estimated by the method of least squares (7, 53).

Block Schemes

Block schemes of all of the stages involved in the SAI-PAI estimation are described in Figs. A3 and A4. A modeling stage has been devised to establish the combination and structure of the base functions attributed to either the sympathetic or parasympathetic activity. On a real set of heartbeats, given such a modeling structure as specified in *Eq. 1*, the estimation of model-defined parameters (g_{1s}, g_{1p}) can be updated along the time using the most efficient and popular methods reported in the literature for recursive parameter estimation (Kalman filtering, point processes, recursive least squares, etc.). A final step linearly combines the time-varying estimation using the disentangling coefficients Ψ_s, Ψ_p to yield the final SAI and PAI measures. The block scheme reported in Fig. A4 has to be considered as an in-depth look of the block "Modeling and Multiple Regression" in Fig. A3. Here, heartbeat data gathered during sympathetic activity only (parasympathetic blockade), and during sympathetic activity only (parasympathetic blockade), both in a supine resting phase and a standing

Table A4. *Results from the rest-fast tilt-table experimental data set*

Statistical Index	Model	Rest	Titl-Table Fast	*P* Value
μ_{RR}, ms	AR_{PP}	881.03 ± 94.55	776.18 ± 66.49	0.004627
	ARL_{PP}	883.03 ± 95.78	774.62 ± 54.46	0.005068
	AR	860.50 ± 80.48	777.18 ± 51.58	0.009375
σ_{RR}, ms	AR_{PP}	21.68 ± 8.02	16.33 ± 4.00	0.064190
	ARL_{PP}	22.18 ± 8.31	16.92 ± 4.51	0.073844
	AR	48.20 ± 9.40	46.00 ± 15.01	0.318951
Sympathetic activity	$LF(AR_{PP})$	476.41 ± 285.63	349.72 ± 203.75	0.303830
	$LF(ARL_{PP})$	568.28 ± 299.64	504.37 ± 269.77	0.704000
	LF(AR)	401.86 ± 330.31	338.33 ± 278.42	0.739734
	$SAI_{NEW(0)}$	10.14 ± 1.30	12.21 ± 1.43	0.002616
	$SAI_{NEW(1)}$	9.51 ± 0.50	12.95 ± 2.07	0.013986
	$SAI_{NEW(2)}$	9.33 ± 0.50	10.70 ± 0.49	0.000156
	$SAI_{NEW(3)}$	33.70 ± 5.42	41.42 ± 3.33	0.002173
	$SAI_{NEW(4)}$	31.80 ± 2.21	36.79 ± 1.85	0.000870
Parasympathetic activity	$HF(AR_{PP})$	214.90 ± 159.75	123.14 ± 79.59	0.103231
	$HF(ARL_{PP})$	239.12 ± 177.12	203.04 ± 102.98	0.815000
	HF(AR)	296.05 ± 153.27	136.80 ± 59.81	0.023688
	$PAI_{NEW(0)}$	10.77 ± 0.81	8.17 ± 1.90	0.001019
	$PAI_{NEW(1)}$	11.59 ± 0.91	8.56 ± 1.48	0.002331
	$PAI_{NEW(2)}$	11.69 ± 1.39	10.46 ± 0.67	0.027591
	$PAI_{NEW(3)}$	39.13 ± 3.15	34.12 ± 1.84	0.002259
	$PAI_{NEW(4)}$	35.89 ± 2.95	30.62 ± 1.58	0.002000
Sympathovagal balance	$LF/HF(AR_{PP})$	2.05 ± 1.57	1.96 ± 1.26	0.753865
	$LF/HF(ARL_{PP})$	1.82 ± 1.43	1.56 ± 0.65	0.977000
	LF/HF(AR)	0.93 ± 0.46	1.51 ± 1.10	0.116943
	$SAI/PAI_{NEW(0)}$	0.83 ± 0.35	1.74 ± 0.47	0.000612
	$SAI/PAI_{NEW(1)}$	0.85 ± 0.18	1.57 ± 0.31	0.011072
	$SAI/PAI_{NEW(2)}$	0.84 ± 0.16	1.03 ± 0.07	0.000977
	$SAI/PAI_{NEW(3)}$	0.94 ± 0.22	1.25 ± 0.13	0.000704
	$SAI/PAI_{NEW(4)}$	0.87 ± 0.13	1.21 ± 0.13	0.000263
RMSSD, ms		28.70 ± 11.32	18.10 ± 3.60	0.038235
pNN50, %		6.54 ± 6.18	1.14 ± 1.14	0.018120
HRV_tri_ind		8.49 ± 2.00	6.50 ± 0.93	0.062213
TINN, ms		182.50 ± 60.00	140.00 ± 45.00	0.160440

Values are median absolute deviation ± SE. *P* values are obtained from the rank-sum test between the rest and fast-tilt sessions. AR, estimates from linear autoregressive model; AR_{PP}, estimates from linear point-process method; ARL_{PP}, estimates from linear point-process method with Laguerre expansion; HF, high frequency; HRV_tri_ind, HRV triangular index; LF, low frequency; LF/HF, ratio of LF to HF; NEW(0), a multiple linear regression using subject-specific (i.e., performed for each subject) recording from one rest-upright condition; NEW(1), a multiple linear regression using subject-specific (i.e., performed for each subject) recording averaging Ψ_S and Ψ_P estimates from stand-up, slow, and fast-tilting conditions; NEW(2), a multiple linear regression using general values (i.e., calculated over all of the subjects), averaging Ψ_S and Ψ_P estimates from stand-up, slow- and fast-tilting conditions, following a leave-one-subject-out procedure; NEW(3), a multiple linear regression using general values (i.e., calculated over all of the subjects) averaging Ψ_S and Ψ_P estimates from the rest-tilt control session of an independent data set; NEW(4), a multiple linear regression using general values (i.e., calculated over all of the subjects) averaging Ψ_S and Ψ_P from subjects of an independent data set undergoing autonomic blockade (parasympathetic suppression → sympathetic kernels Ψ_S; sympathetic suppression → parasympathetic kernels Ψ_P); PAI, parasympathetic activity index; pNN50, the proportion derived by dividing the number of interval differences of successive NN intervals >50 ms by the total number of NN intervals; RMSSD, root mean square of the successive differences; SAI, sympathetic activity index; SAI/PAI, ratio of SAI to PAI; TINN; triangular interpolation of NN interval histogram; μ_{RR}, estimated mean R-R interval; σ_{RR}, standard deviation of the R-R intervals.

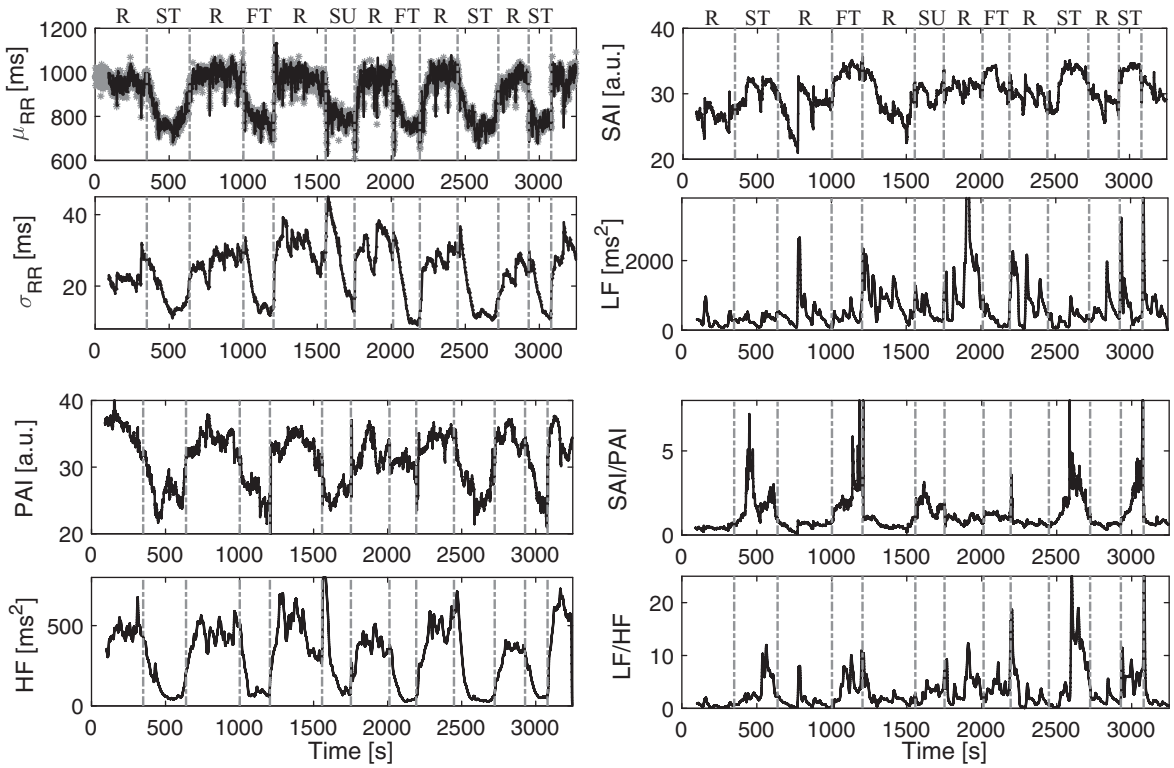

Fig. A5. Instantaneous heartbeat statistics computed from an exemplary subject of the tilt-table protocol. *Top left*: the estimated mean R-R interval at time t, $\mu_{RR}(t)$, superimposed on the recorded R-R series, and the instantaneous heartbeat standard deviation at time t, $\sigma_{RR}(t)$, are shown. Instantaneous sympathetic and parasympathetic activity, and sympathovagal balance as estimated through sympathetic activity index (SAI) and parasympathetic activity index (PAI), and ratio of SAI to PAI (SAI/PAI) measures, along with the low frequency (LF), high frequency (HF), and ratio of LF to HF (LF/HF) are shown in the other panels. Vertical dotted lines indicate the beginning and end of each experimental transition. For this subject, the first transition is from rest (R) to slow tilt (ST) and back, the second is from R to fast tilt (FT) and back, the third and fourth are from R to stand-up (SU), then R to ST, and the final R to FT and back. Transitions are randomized for each subject. a.u., Arbitrary units.

tilting phase, were considered as reference heartbeat data. For each of these data sets, after fitting an AR model with Laguerre expansion of the terms, a multiple-regression stage considering desired changes (e.g., increase of the sympathetic activity during tilt with respect to rest) has been performed for each subject. Then, coefficients of general applicability Ψ_s, Ψ_p were obtained through the average among subjects.

Experimental Results

Goodness of fit analysis. Table A1 shows results from a comprehensive goodness-of-fit analysis performed on the tilt-table protocol, as well as the LBNP and handgrip protocols. Specifically, we show intersubject statistics summarized as interval (median ± MAD), minimum and maximum values on the sum of the squared distances of the points outside the confidence interval of the autocorrelation plot, as well as KS distance.

Tilt-table protocol. To demonstrate how the proposed SAI and PAI measures are able to follow sympathetic and parasympathetic changes, respectively, at a single-subject level, SAI-PAI estimates along with their LF-HF counterpart, as well as standard instantaneous heartbeat statistics in the time domain, are reported here in Tables A2, A3, and A4. See Figs. A5, and A6.

Tables A2, A3, and A4 show comprehensive results gathered from three estimation methodologies: linear point-process method (AR_{PP}), linear point-process method with Laguerre expansion (ARL_{PP}), and standard linear AR modeling. Through each of these methods, considering rest-to-stand-up (Table A2), rest-to-slow-tilt (Table A4), and rest-to-fast-tilt (Table A3) procedures, the following heartbeat dynamics measures were evaluated: mean R-R interval (μ_{RR}), standard deviation of the R-R intervals (σ_{RR}), sympathetic and parasympathetic activity, and sympathovagal balance.

Table A1 shows similar performances between the three modeling methods while discerning rest from stand-up sessions using μ_{RR} and σ_{RR} estimates. The same applies for the estimation of LF, HF, and LF/HF. Nevertheless, the use of ARL_{PP} modeling for the estimation of SAI, PAI, and SAI/PAI measures significantly outperform the use of AR_{PP} and AR modeling for the identification of sympathetic and parasympathetic activities. All SAI and PAI estimates are associated with significant differences between rest and stand-up sessions with P values as low as $<10^{-5}$.

Table A3 also shows similar performances between the three modeling methods while discerning rest from slow-tilt sessions using μ_{RR}, σ_{RR}, LF, HF, and LF/HF. All SAI and PAI estimates are associated with significant differences between rest and stand-up sessions with P values as low as $<10^{-3}$.

Table A4 also shows similar performances between the three modeling methods while discerning rest from fast-tilt sessions using μ_{RR}, σ_{RR}, LF, HF, and LF/HF. All SAI and PAI estimates are associated with significant differences between rest and stand-up sessions with P values as low as $<10^{-3}$.

Autonomic blockade

For the sake of completeness, we here report results and related statistics (median ± MAD) considering postural changes during control and sympathetic/parasympathetic blockades, following a previously validated approach described in Schetzen (42).

During the control postural changes, SAI and PAI estimates, along with their ratio, follow physiologically plausible trends (i.e., SAI

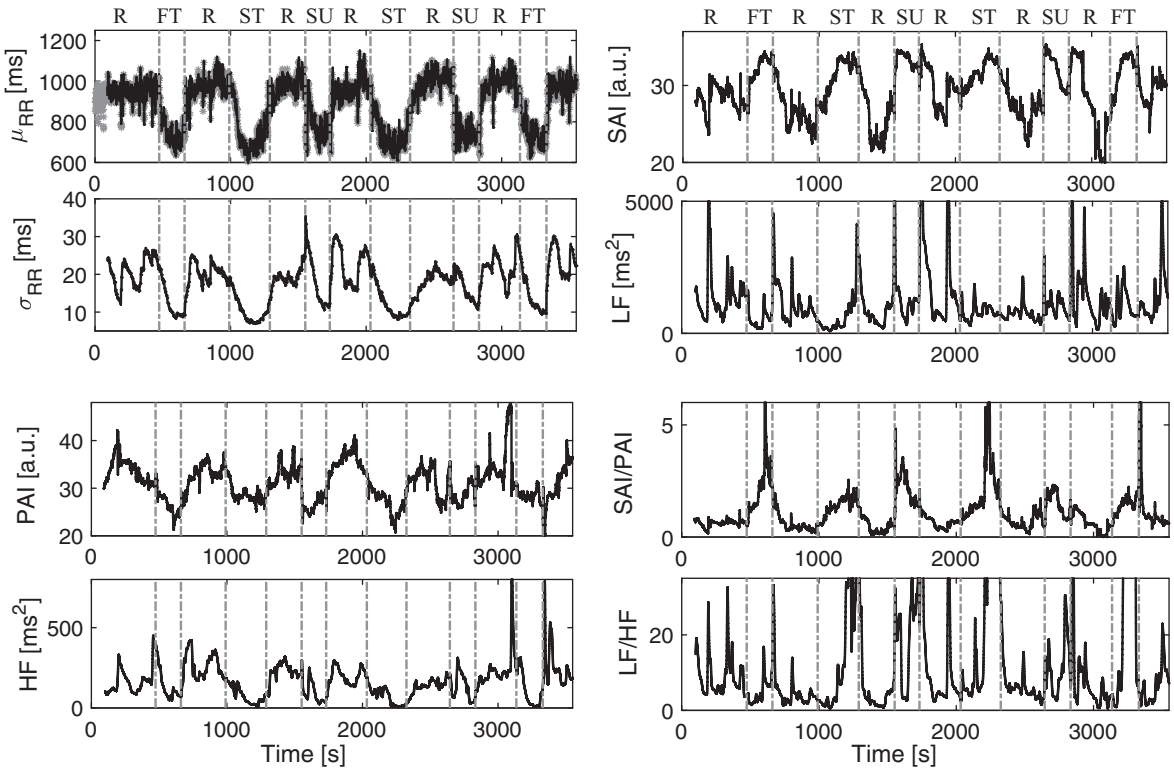

Fig. A6. Instantaneous heartbeat statistics computed from an exemplary subject of the tilt-table protocol. *Top left*: the estimated mean R-R interval at time t, $\mu_{RR}(t)$, superimposed on the recorded R-R series, and the instantaneous heartbeat standard deviation at time t, $\sigma_{RR}(t)$, are shown. Instantaneous sympathetic and parasympathetic activity, and sympathovagal balance as estimated through sympathetic activity index (SAI) and parasympathetic activity index (PAI), and ratio of SAI to PAI (SAI/PAI) measures, along with the low frequency (LF), high frequency (HF), and ratio of LF to HF (LF/HF) are shown in the other panels. Vertical dotted lines indicate the beginning and end of each experimental transition. For this subject, the first transition is from rest (R) to fast tilt (FT) and back, the second is from R to slow tilt (ST) and back, the third is from R to stand up (SU), then R to ST, R to SU, and R to FT and back. Transitions are randomized for each subject. a.u., Arbitrary units.

increases after standing with respect to rest; PAI decreases after standing with respect to rest). As expected, autonomic blockades make SAI and PAI reaching relative minimum and maximal values. Specifically, the PAI is at a minimum in the upright + atropine case (i.e., parasympathetic blockade after standing) and at maximum in the supine + propanolol case (i.e., resting state during sympathetic blockade), whereas the SAI is at a maximum in the control standing case, and at a minimum in the supine + propranolol case (i.e., resting state during sympathetic blockade). Consistently, the sympathovagal balance SAI/PAI is at minimum in the supine + propanolol case (i.e., resting state during sympathetic blockade), and at maximum in the upright + atropine case (i.e., parasympathetic blockade after standing). See Table A5.

ACKNOWLEDGMENTS

The authors are grateful to Roger G. Mark and Thomas Heldt (Harvard-MIT Division of Health Sciences and Technology, Cambridge, MA) for kindly providing the tilt-table data, and to Vegard Bruun Wyller (Rikshospitalet University Hospital, Oslo, Norway) for kindly providing the lower body negative pressure and handgrip data analyzed in this study.

GRANTS

This study received partial funding from the Department of Anesthesia, Critical Care and Pain Medicine, Massachusetts General Hospital, Harvard Medical School, Boston, MA.

DISCLOSURES

An International Application (PCT/US2016/044844) was filed on July 29, 2016 for the method described in this paper.

AUTHOR CONTRIBUTIONS

G.V., L.C., and R.B. conceived and designed research; G.V., L.C., and R.B. analyzed data; G.V., L.C., J.P.S., and R.B. interpreted results of experiments; G.V. and R.B. prepared figures; G.V., L.C., J.P.S., and R.B. drafted manuscript; G.V., L.C., J.P.S., and R.B. edited and revised manuscript; G.V., L.C., J.P.S., and R.B. approved final version of manuscript.

Table A5. *Results from the autonomic blockade protocol*

	Control Test, No Drugs (n = 14 Subjects)			Control and Autonomic Blockade (n = 7 + 7 Subjects)	
Autonomic Index	Rest	Standing	*P* Value	Control/Propranorol, Rest	Control/Athropine, Standing
SAI, AU	40.010 ± 2.046	42.569 ± 1.339	0.001	34.921 ± 1.086	43.668 ± 2.342
PAI, AU	30.308 ± 1.243	28.544 ± 1.218	0.048	30.825 ± 1.08	23.469 ± 4.689
SAI/PAI	1.357 ± 0.156	1.514 ± 0.079	0.024	1.129 ± 0.099	1.667 ± 0.229

Values are median absolute deviation ± SE. *P* values are from the sign-rank nonparametric test for paired data. PAI, parasympathetic activity index; SAI, sympathetic activity index; SAI/PAI, ratio of SAI to PAI.</.>

REFERENCES

1. **Akselrod S.** Components of heart rate variability: basic studies. In: *Heart Rate Variability*, edited by Malik M, Camm AJ. Hoboken, NJ: Wiley-Blackwell, 1995, p. 147–163.
2. **Akselrod S, Gordon D, Madwed JB, Snidman NC, Shannon DC, Cohen RJ.** Hemodynamic regulation: investigation by spectral analysis. *Am J Physiol Heart Circ Physiol* 249: H867–H875, 1985. doi:10.1152/ajpheart.1985.249.4.H867.
3. **Akselrod S, Gordon D, Ubel FA, Shannon DC, Berger AC, Cohen RJ.** Power spectrum analysis of heart rate fluctuation: a quantitative probe of beat-to-beat cardiovascular control. *Science* 213: 220–222, 1981. doi:10.1126/science.6166045.
4. **Andersen P.** *Statistical Models Based on Counting Processes*. New York: Springer Verlag, 1993. doi:10.1007/978-1-4612-4348-9.
5. **Armoundas AA, Chon KH.** *Method and Apparatus for Detection and Treatment of Autonomic System Imbalance*. US Patent App. No. 12/373,227. July 6, 2007.
6. **Barbieri R, Brown EN.** Analysis of heartbeat dynamics by point process adaptive filtering. *IEEE Trans Biomed Eng* 53: 4–12, 2006. doi:10.1109/TBME.2005.859779.
7. **Barbieri R, Matten EC, Alabi AA, Brown EN.** A point-process model of human heartbeat intervals: new definitions of heart rate and heart rate variability. *Am J Physiol Heart Circ Physiol* 288: H424–H435, 2005. doi:10.1152/ajpheart.00482.2003.
8. **Batzel J, Baselli G, Mukkamala R, Chon KH.** Modelling and disentangling physiological mechanisms: linear and nonlinear identification techniques for analysis of cardiovascular regulation. *Philos Trans A Math Phys Eng Sci* 367: 1377–1391, 2009. doi:10.1098/rsta.2008.0266.
9. **Berger RD, Saul JP, Cohen RJ.** Transfer function analysis of autonomic regulation. I. Canine atrial rate response. *Am J Physiol Heart Circ Physiol* 256: H142–H152, 1989. doi:10.1152/ajpheart.1989.256.1.H142.
10. **Chen X, Mukkamala R.** Selective quantification of the cardiac sympathetic and parasympathetic nervous systems by multisignal analysis of cardiorespiratory variability. *Am J Physiol Heart Circ Physiol* 294: H362–H371, 2008. doi:10.1152/ajpheart.01061.2007.
11. **Chen Z, Brown EN, Barbieri R.** Assessment of autonomic control and respiratory sinus arrhythmia using point process models of human heart beat dynamics. *IEEE Trans Biomed Eng* 56: 1791–1802, 2009. doi:10.1109/TBME.2009.2016349.
12. **Chen Z, Purdon PL, Harrell G, Pierce ET, Walsh J, Brown EN, Barbieri R.** Dynamic assessment of baroreflex control of heart rate during induction of propofol anesthesia using a point process method. *Ann Biomed Eng* 39: 260–276, 2011. doi:10.1007/s10439-010-0179-z.
13. **Citi L, Brown EN, Barbieri R.** A real-time automated point-process method for the detection and correction of erroneous and ectopic heartbeats. *IEEE Trans Biomed Eng* 59: 2828–2837, 2012. doi:10.1109/TBME.2012.2211356.
14. **Esler M, Rumantir M, Wiesner G, Kaye D, Hastings J, Lambert G.** Sympathetic nervous system and insulin resistance: from obesity to diabetes. *Am J Hypertens* 14: 304S–309S, 2001. doi:10.1016/S0895-7061(01)02236-1.
15. **Floras JS, Legault L, Morali GA, Hara K, Blendis LM.** Increased sympathetic outflow in cirrhosis and ascites: direct evidence from intraneural recordings. *Ann Intern Med* 114: 373–380, 1991. doi:10.7326/0003-4819-114-5-373.
16. **Goldstein DS, Bentho O, Park MY, Sharabi Y.** Low-frequency power of heart rate variability is not a measure of cardiac sympathetic tone but may be a measure of modulation of cardiac autonomic outflows by baroreflexes. *Exp Physiol* 96: 1255–1261, 2011. doi:10.1113/expphysiol.2010.056259.
17. **Grassi G.** Role of the sympathetic nervous system in human hypertension. *J Hypertens* 16, *Suppl*: 1979–1987, 1998. doi:10.1097/00004872-199816121-00019.
18. **Grassi G, Esler M.** How to assess sympathetic activity in humans. *J Hypertens* 17: 719–734, 1999. doi:10.1097/00004872-199917060-00001.
19. **Heldt T, Oefinger MB, Hoshiyama M, Mark RG.** Circulatory response to passive and active changes in posture. *Comput Cardiol* 30: 263–266, 2003. doi:10.1109/CIC.2003.1291141.
20. **Heldt T, Shim EB, Kamm RD, Mark RG.** Computational modeling of cardiovascular response to orthostatic stress. *J Appl Physiol (1985)* 92: 1239–1254, 2002. doi:10.1152/japplphysiol.00241.2001.
21. **Hirsch JA, Bishop B.** Respiratory sinus arrhythmia in humans: how breathing pattern modulates heart rate. *Am J Physiol Heart Circ Physiol* 241: H620–H629, 1981. doi:10.1152/ajpheart.1981.241.4.H620.
22. **Houle MS, Billman GE.** Low-frequency component of the heart rate variability spectrum: a poor marker of sympathetic activity. *Am J Physiol Heart Circ Physiol* 276: H215–H223, 1999. doi:10.1152/ajpheart.1999.276.1.H215.
23. **Kamath MV, Fallen EL.** Power spectral analysis of heart rate variability: a noninvasive signature of cardiac autonomic function. *Crit Rev Biomed Eng* 21: 245–311, 1993.
24. **Kaye DM, Lambert GW, Lefkovits J, Morris M, Jennings G, Esler MD.** Neurochemical evidence of cardiac sympathetic activation and increased central nervous system norepinephrine turnover in severe congestive heart failure. *J Am Coll Cardiol* 23: 570–578, 1994. doi:10.1016/0735-1097(94)90738-2.
25. **Levy MN.** Sympathetic-parasympathetic interactions in the heart. *Circ Res* 29: 437–445, 1971. doi:10.1161/01.RES.29.5.437.
26. **Malliani A.** Association of heart rate variability components with physiological regulatory mechanisms. In: *Heart Rate Variability*, edited by Malik M, Camm AJ. Hoboken, NJ: Wiley-Blackwell, 1995, p. 173–188.
27. **Malliani A.** Cardiovascular variability is/is not an index of autonomic control of circulation. *J Appl Physiol (1985)* 101: 684–688, 2006. doi:10.1152/japplphysiol.00562.2006.
28. **Malpas SC.** Neural influences on cardiovascular variability: possibilities and pitfalls. *Am J Physiol Heart Circ Physiol* 282: H6–H20, 2002. doi:10.1152/ajpheart.2002.282.1.H6.
29. **Mancia G, Grassi G.** The autonomic nervous system and hypertension. *Circ Res* 114: 1804–1814, 2014. doi:10.1161/CIRCRESAHA.114.302524.
30. **Marmarelis VZ.** Identification of nonlinear biological systems using Laguerre expansions of kernels. *Ann Biomed Eng* 21: 573–589, 1993. doi:10.1007/BF02368639.
31. **McCrory C, Berkman LF, Nolan H, O'Leary N, Foley M, Kenny RA.** Speed of heart rate recovery in response to orthostatic challenge: novelty and significance. *Circ Res* 119: 666–675, 2016. doi:10.1161/CIRCRESAHA.116.308577.
32. **Mitsis GD, Zhang R, Levine BD, Marmarelis VZ.** Modeling of nonlinear physiological systems with fast and slow dynamics. II. Application to cerebral autoregulation. *Ann Biomed Eng* 30: 555–565, 2002. doi:10.1114/1.1477448.
33. **Miyakawa K, Koepchen HP, Polosa C.** History of studies and concepts of blood pressure waves. In: *Mechanisms of Blood Pressure Waves*. Berlin: Japan Scientific Societies, 1984, p. 3–23.
34. **Parati G, Esler M.** The human sympathetic nervous system: its relevance in hypertension and heart failure. *Eur Heart J* 33: 1058–1066, 2012. doi:10.1093/eurheartj/ehs041.
35. **Pomeranz B, Macaulay RJ, Caudill MA, Kutz I, Adam D, Gordon D, Kilborn KM, Barger AC, Shannon DC, Cohen RJ, Benson H.** Assessment of autonomic function in humans by heart rate spectral analysis. *Am J Physiol Heart Circ Physiol* 248: H151–H153, 1985. doi:10.1152/ajpheart.1985.248.1.H151.
36. **Posada-Quintero HF, Florian JP, Orjuela-Cañón AD, Aljama-Corrales T, Charleston-Villalobos S, Chon KH.** Power spectral density analysis of electrodermal activity for sympathetic function assessment. *Ann Biomed Eng* 44: 3124–3135, 2016. doi:10.1007/s10439-016-1606-6.
37. **Rajendra Acharya U, Paul Joseph K, Kannathal N, Lim CM, Suri JS.** Heart rate variability: a review. *Med Biol Eng Comput* 44: 1031–1051, 2006. doi:10.1007/s11517-006-0119-0.
38. **Reyes del Paso GA, Langewitz W, Mulder LJ, van Roon A, Duschek S.** The utility of low frequency heart rate variability as an index of sympathetic cardiac tone: a review with emphasis on a reanalysis of previous studies. *Psychophysiology* 50: 477–487, 2013. doi:10.1111/psyp.12027.
39. **Sassi R, Cerutti S, Lombardi F, Malik M, Huikuri HV, Peng CK, Schmidt G, Yamamoto Y, Gorenek B, Lip GH, Grassi G, Kudaiberdieva G, Fisher JP, Zabel M, Macfadyen R.** Advances in heart rate variability signal analysis: joint position statement by the e-Cardiology ESC Working Group and the European Heart Rhythm Association co-endorsed by the Asia Pacific Heart Rhythm Society. *Europace* 17: 1341–1353, 2015. doi:10.1093/europace/euv015.
40. **Saul JP, Berger RD, Albrecht P, Stein SP, Chen MH, Cohen RJ.** Transfer function analysis of the circulation: unique insights into cardiovascular regulation. *Am J Physiol Heart Circ Physiol* 261: H1231–H1245, 1991. doi:10.1152/ajpheart.1991.261.4.H1231.

42. **Schetzen M.** *The Volterra and Wiener Theories of Nonlinear Systems*. Malabar, FL: Krieger, 1980.
43. **Schwartz P, De Ferrari G.** Sympathetic-parasympathetic interaction in health and disease: abnormalities and relevance in heart failure. *Heart Fail Rev* 16 101–107, 2010.10.1007/s10741-010-9179-1.
44. **Sinski M, Lewandowski J, Abramczyk P, Narkiewicz K, Gaciong Z.** Why study sympathetic nervous system? *J Physiol Pharmacol* 57, *Suppl* 11: 79–92, 2006.
45. **Sunagawa K, Kawada T, Nakahara T.** Dynamic nonlinear vago-sympathetic interaction in regulating heart rate. *Heart Vessels* 13: 157–174, 1998. doi:10.1007/BF01745040.
46. **Tahsili-Fahadan P, Geocadin RG.** Heart-brain axis: effects of neurologic injury on cardiovascular function. *Circ Res* 120: 559–572, 2017. doi:10.1161/CIRCRESAHA.116.308446.
47. **Task Force of the European Society of Cardiology and the North American Society of Pacing and Electrophysiology.** Heart rate variability: standards of measurement, physiological interpretation and clinical use. *Circulation* 93: 1043–1065, 1996. doi:10.1161/01.CIR.93.5.1043.
48. **Taylor JA, Carr DL, Myers CW, Eckberg DL.** Mechanisms underlying very-low-frequency RR-interval oscillations in humans. *Circulation* 98: 547–555, 1998. doi:10.1161/01.CIR.98.6.547.
49. **Treskes RW, van der Velde ET, Barendse R, Bruining N.** Mobile health in cardiology: a review of currently available medical apps and equipment for remote monitoring. *Expert Rev Med Devices* 13: 823–830, 2016. doi:10.1080/17434440.2016.1218277.
50. **Ursino M, Magosso E.** Role of short-term cardiovascular regulation in heart period variability: a modeling study. *Am J Physiol Heart Circ Physiol* 284: H1479–H1493, 2003. doi:10.1152/ajpheart.00850.2002.
51. **Valenza G, Citi L, Barbieri R.** Estimation of instantaneous complex dynamics through Lyapunov exponents: a study on heartbeat dynamics. *PLoS One* 9: e105622, 2014. doi:10.1371/journal.pone.0105622.
52. **Valenza G, Citi L, Lanatá A, Scilingo EP, Barbieri R.** Revealing real-time emotional responses: a personalized assessment based on heartbeat dynamics. *Sci Rep* 4: 4998, 2014. doi:10.1038/srep04998.
53. **Valenza G, Citi L, Scilingo EP, Barbieri R.** Point-process nonlinear models with Laguerre and Volterra expansions: Instantaneous assessment of heartbeat dynamics. *IEEE Trans Signal Process* 61: 2914–2926, 2013. doi:10.1109/TSP.2013.2253775.
54. **Valenza G, Citi L, Scilingo EP, Barbieri R.** Inhomogeneous point-process entropy: an instantaneous measure of complexity in discrete systems. *Phys Rev E Stat Nonlin Soft Matter Phys* 89: 052803, 2014. doi:10.1103/PhysRevE.89.052803.
55. **Valenza G, Orsolini S, Diciotti S, Citi L, Scilingo EP, Guerrisi M, Danti S, Lucetti C, Tessa C, Barbieri R, Toschi N.** Assessment of spontaneous cardiovascular oscillations in parkinson's disease. *Biomed Signal Process Control* 26: 80–89, 2016. doi:10.1016/j.bspc.2015.12.001.
56. **Vaz M, Jennings G, Turner A, Cox H, Lambert G, Esler M.** Regional sympathetic nervous activity and oxygen consumption in obese normotensive human subjects. *Circulation* 96: 3423–3429, 1997. doi:10.1161/01.CIR.96.10.3423.
57. **Veith RC, Lewis N, Linares OA, Barnes RF, Raskind MA, Villacres EC, Murburg MM, Ashleigh EA, Castillo S, Peskind ER, et al.** Sympathetic nervous system activity in major depression. Basal and desipramine-induced alterations in plasma norepinephrine kinetics. *Arch Gen Psychiatry* 51: 411–422, 1994. doi:10.1001/archpsyc.1994.03950050071008.
58. **Vetter R, Vesin JM, Celka P, Scherrer U.** Observer of the human cardiac sympathetic nerve activity using noncausal blind source separation. *IEEE Trans Biomed Eng* 46: 322–330, 1999. doi:10.1109/10.748985.
59. **Vetter R, Virag N, Vesin JM, Celka P, Scherrer U.** Observer of autonomic cardiac outflow based on blind source separation of ECG parameters. *IEEE Trans Biomed Eng* 47: 578–582, 2000. doi:10.1109/10.841328.
60. **Wac K.** Smartphone as a personal, pervasive health informatics services platform: literature review. *Yearb Med Inform* 7: 83–93, 2012.
61. **Wyller VB, Barbieri R, Saul JP.** Blood pressure variability and closed-loop baroreflex assessment in adolescent chronic fatigue syndrome during supine rest and orthostatic stress. *Eur J Appl Physiol* 111: 497–507, 2011. doi:10.1007/s00421-010-1670-9.
62. **Wyller VB, Saul JP, Barbieri R, de Lange C, Hopp E, Norum IB, Thaulow E.** Autonomic heart rate control at rest and during unloading of the right ventricle in repaired tetralogy of Fallot in adolescents. *Am J Cardiol* 102: 1085–1089, 2008. doi:10.1016/j.amjcard.2008.05.065.
63. **Xiao X, Mukkamala R, Cohen R.** A selective quantification of cardiac sympathetic and parasympathetic control and its validation through pharmacological blockade. In: *Computers in Cardiology*, Chicago, IL, September 19–22, 2004, p. 477–480. doi:10.1109/CIC.2004.1442978.
64. **Xiao X, Mukkamala R, Sheynberg N, Grenon SM, Ehrman MD, Mullen TJ, Ramsdell CD, Williams GH, Cohen RJ.** Effects of simulated microgravity on closed-loop cardiovascular regulation and orthostatic intolerance: analysis by means of system identification. *J Appl Physiol (1985)* 96: 489–497, 2004. doi:10.1152/japplphysiol.00602.2003.
65. **Yasuma F, Hayano J.** Respiratory sinus arrhythmia: why does the heartbeat synchronize with respiratory rhythm? *Chest* 125: 683–690, 2004. doi:10.1378/chest.125.2.683.
66. **Zhong Y, Jan KM, Ju KH, Chon KH.** Quantifying cardiac sympathetic and parasympathetic nervous activities using principal dynamic modes analysis of heart rate variability. *Am J Physiol Heart Circ Physiol* 291: H1475–H1483, 2006. doi:10.1152/ajpheart.00005.2006.
67. **Zhong Y, Wang H, Ju KH, Jan KM, Chon KH.** Nonlinear analysis of the separate contributions of autonomic nervous systems to heart rate variability using principal dynamic modes. *IEEE Trans Biomed Eng* 51: 255–262, 2004. doi:10.1109/TBME.2003.820401.
68. **Zong W, Moody G.** *WQRS-single-channel QRS detector based on length transform* (Online). Physionet. http://www.physionet.org/physiotools/wag/wqrs-1.htm [4 May 2018].